*vehicles*

MDPI

*Article*

# Investigation of the Causes of Railway Track Gauge Narrowing

**Péter Bocz [1], Nándor Liegner [1], Ákos Vinkó [1] and Szabolcs Fischer [2,*]**

[1] Department of Highway and Railway Engineering, Faculty of Civil Engineering, Budapest University of Technology and Economics, 1111 Budapest, Hungary; bocz.peter@emk.bme.hu (P.B.);liegner.nandor@emk.bme.hu (N.L.); vinko.akos@emk.bme.hu (Á.V.)
[2] Department of Transport Infrastructure and Water Resources Engineering, Faculty of Architecture, Civil and Transport Engineering, Széchenyi István University, 9026 Győr, Hungary
* Correspondence: fischersz@sze.hu; Tel.: +36-(96)-613-544

**Abstract:** On behalf of MÁV Hungarian State Railways Ltd., the authors carried out a research and development (R&D) project on behalf of the Budapest University of Technology and Economics, Department of Highway and Railway Engineering, on the subject of "Research and investigation of the causes of gauge narrowing by finite-element modeling in running track and turnout, and under operational and laboratory conditions". The main objective of the research was to investigate the causes of localized defects of gauge narrowing in railway tracks based on machine and manual track measurements, laboratory measurements, and theoretical considerations. The measures proposed as a consequence of identifying the causes could significantly contribute to reducing the number and extent of local defects in the future. Furthermore, the research aims to develop new theories in less scientifically mature areas and provide procedures and instructions that professional engineers and practitioners can easily apply. The main areas of research, which are not exhaustive, are as follows: (i) the evaluation of the measurement results provided by track geometry measuring and recording cars; (ii) on-site investigations in the railway track in terms of gauge and rail profile measurements; and, based on these, (iii) the selection of concrete sleepers, which were removed from the track and subjected to more detailed geometrical investigations in the laboratory, together with the components of the rail reinforcement; (iv) the track–vehicle connection, tight running in straight and curved track sections under track confinement; (v) modeling of the stability and deflection of the rail when the rail fastenings lose part of their supporting function; and (vi) finite element modeling of the concrete sleepers under operating conditions such as slow deformation of the concrete, temperature variation effects, and lateral support on the ballast. In the already-narrowed track section, the tight vehicle running is not the cause of the track gauge narrowing but a consequence, so it is not investigated in this paper.

**Keywords:** railway track; track gauge; track gauge narrowing; plain track; turnout; statistical analysis; finite element modeling

check for updates

**Citation:** Bocz, P.; Liegner, N.; Vinkó, Á.; Fischer, S. Investigation of the Causes of Railway Track Gauge Narrowing. *Vehicles* **2023**, *5*, 949–977. https://doi.org/10.3390/vehicles5030052

Academic Editors: Pedro Antunes, Hugo Magalhães and Pedro Aires Montenegro

Received: 2 June 2023
Revised: 28 July 2023
Accepted: 7 August 2023
Published: 10 August 2023

**Copyright:** © 2023 by the authors. Licensee MDPI, Basel, Switzerland. This article is an open access article distributed under the terms and conditions of the Creative Commons Attribution (CC BY) license (https://creativecommons.org/licenses/by/4.0/).

## 1. Introduction

### 1.1. General Introduction

Transport includes land, sea, and air transport [1–3]. Air and space transit should be combined in the discussion of the topic.

Transportation has always been an important part of human society, allowing people, products, and services to move from one location to another. From early human migration to the modern global economy, the necessity for transportation has developed throughout time.

Walking was the original mode of ground transportation, utilized for thousands of years. Later, humans tamed animals such as horses, camels, and oxen to aid in transporting goods and people. Carts and chariots were developed with the invention of the wheel in ancient Mesopotamia, leading to the earliest road networks.

The 18th and 19th centuries saw considerable developments in transportation as a result of the Industrial Revolution. The invention of steam-powered vehicles, such as trains and steamboats, transformed transportation and commerce.

The Wright brothers' aircraft made the first successful powered flight in 1903. Air travel grew increasingly popular in the twentieth century, and it is now the quickest option to travel great distances. As a result, air travel has significantly influenced worldwide commerce, tourism, and globalization.

The first satellite was sent into orbit in 1957; space transportation is a relatively new invention. Since then, people's flights to the moon and spacecraft launched to study other planets have extended space exploration. As a result, space travel has been critical in scientific study, the military, and communication.

For thousands of years, boats and ships have been used for fishing, commerce, and warfare. However, the invention of steam-powered ships in the nineteenth century changed ocean and river transportation. Ships are now the principal form of transportation for bulk commodities like oil and grain.

Land transport since antiquity requires roads, ports, and docks [4–8]. Modern innovations also necessitated trains and airports [1–3,9–12]. Logistics, along with transport, became crucial [13–17].

The current article discusses the details of railway track gauges, i.e., the track gauge narrowing. The evolution of fixed-rail transportation is beneficial to introduce the issue and establish its topicality. In the mining business, wagon tracks were the first fixed-rail tracks. After "horse-drawn locomotives," George Stephenson invented the steam locomotive. In 1825, the Stockton–Darlington became the first steam railway. Steam locomotives transformed rail transit.

George Stephenson's Rocket, the "official" first steam locomotive, had a track gauge of 1422 mm (4 feet 8 inches) and was eventually extended by 13 mm. It favored wheel flange lateral forces [1].

It may have been the Roman road vehicle track gauge, according to Pompeii and other discoveries. Everything was measured then. Two persons might easily sit on each side of a corridor at 1435 mm [1].

The gauge value has covered 1435 mm, the nominal track gauge, for decades.

In cross-section, the track gauge is the shortest distance between the rail heads' inner guiding edges in the plane parallel to the rail heads' top tangent. The considered depth below the rail head top tangent ($Z_P$) is 14 mm for Vignol rails and 9 or 10 mm for grooved rails based on EN 13848-1 [18].

To be able to achieve the aims of this article, research was conducted into a selection of the global literature on the topic of railroad track gauges. This research was conducted globally, although it could not be thorough or complete due to space constraints. However, an attempt was made to summarize the content deemed most significant and referenced the most often; the results of this endeavor are summarized in the following paragraphs. The authors gathered the papers and organized them according to the following primary topics: (i) the development of track gauges around the world, as well as their distribution and connecting history; (ii) the measurement possibilities of track gauge(s) (it is important to note that only the non-commercial and non-standardized methods are discussed and detailed in the Introduction; the standardized methods are partly discussed in Section 2); (iii) the degradation of track gauges over time; and (iv) the degradation of railway tracks.

### *1.2. Literature Review*

In the following paragraphs, the authors will depict the first group (i) mentioned in Section 1.1. This organization is interested in the evolution of track gauges across the globe, as well as the history of their distribution and relationship.

Czére [1], as well as Chandra and Agarwal [19] discussed the evolution of track gauges in the past in a very detailed manner. The gauge of a railway track considerably influences

a railway system's efficiency and safety. Railway track gauge development has been an extended process covering many decades, with several stages of standardization.

Tzanakakis [20] presents a track gauge creation hypothesis. He begins with Bronze Age vehicles, Roman Empire mythology, and Julius Caesar's traditions. Next, he measures longitudinal tracks and road vehicles' "wheelsets." Finally, British engineers and George Stephenson's locomotive established the standard gauge of 1435 mm and English railroads of comparable construction in the 1800s.

Monfort [21] examines Spanish standard gauge railway construction from 1989 through 2019.

Puffert [22,23] studies track gauge standardization. His book [22] covers North American railways between 1830 and 1890. In the 1830s, several track gauges were used in the US, Canada, and elsewhere. Nine gauge-valued areas were formed by 1860.

Wang et al. [24] examined track gauge dispersion across Eurasia. Eurasia has 11 railway track gauge values: broad, standard, and narrow. 1520, 1435, and 1067 mm are typical. Track gauge coverage and geographical dispersion vary greatly. These may divide rail regimes and networks. Eight rail geosystems resulted, with 1435 and 1520 mm gauge gaps being enormous. China and neighboring nations are quickly building standard gauge railroads. Standard gauge high-speed railroads have recently connected Moscow–Beijing and Beijing–Singapore. However, high-speed trains can only partly link neighboring nations with various track gauges. Technology, route dependence, geopolitics, national security, and military-width colonial terrain impact Eurasia's rail geo-system, which has five geo-modes of rail gauge spreading.

The aforementioned (ii) group (see Section 1.1)—track gauge measurement possibilities—is represented in the following paragraphs. (It must be mentioned that only the non-commercial and non-standardized methods are overviewed and detailed here in the Introduction; the standardized methods have been dealt with in Section 2).

Zheng et al. [25] devised a portable trolley system for evaluating railway track gauge and rail deterioration. The approach uses a laser vision inspection model and system calibration. The method involves three-dimensional machine vision.

Pay et al. [26] devised and built an IoT-DTG (Internet-of-Things-enhanced digital track gauge) to measure track gauge and superelevation. (in other words: cant or cross-level). It has a better measuring capacity and accuracy than manual track gauge measurement devices. The innovative technology saves 50% labor, 60% efficiency, and SGD 19,200 annually (Singapore dollars).

Yilmazer et al. [27] created a drone-based optical and image analysis track gauge measurement system. The drone must fly at a certain height, unaffected by the cars. Image analysis removes vibrations. Gaussian filters and unique detection techniques may identify tracks in photos.

Zhang et al. [28] used wheel and rail transverse motion to estimate track gauge. Two laser sources and two cameras dynamically capture the rail head's inner side. Rail profile dictates parameters. The track gauge is computed using the wheel's lateral displacement and the rail head's laser point's vertical displacement. The experimental findings demonstrate the system's simple hardware architecture, little data calculation, excellent measurement accuracy, and non-contact gauge-spacing measuring.

Shi et al. [29] designed a track-detecting trolley-mounted laser triangulation tracking system. Two 2-D laser scanners collected left- and right-track profile data. An iterative closest-point (ICP) method calibrated sensor data, and an adaptive filter technique smoothed the contour. To be able to increase positioning accuracy, the track gauge was fitted to the rail head curve using least squares. According to studies, the suggested approach enhances track gauge measuring properly and effectively with a $\pm 1$ mm precision.

Tsubokawa and Ishikawa [30] designed railway track measurement equipment that can be installed on a vehicle that measures gauge, twist, and loaded track conditions. Laser-based, non-contact measuring technology "scans" rails in two dimensions at a track cross-section. The maximum measurement speed is 40 km/h. A motor automobile was

measured many times across a 400 m radius curve with a 30 mm superelevation. Four sleepers had their rail fastenings removed to test railway gauge variance. A standard railway wagon was installed to measure a 120 m site radius track segment with 107 mm superelevation and 1067 mm gauge at 10–40 km/h several times. Track gauge repeatability was 0.3 mm, and 5 m base length twist repeatability was 1.0 mm.

Tang et al. [31] used a 2D laser scanner to measure grooved tramway rails. It measures +/–0.6 mm accuracy with the "laser triangulation" technique. Measured rail head profiles were first mathematically filtered. Then, the rail head detection and gauge measurement were lab-tested.

The authors discuss the aforementioned (iii) and (iv) groups (see Section 1.1)—track gauge degradation in fixed-rail applications (tramways, railroads, etc.) and track gauge-specific regions and results—in the following paragraphs.

Németh et al. [12] examined track gauge changes over time on five low-traffic and five high-traffic Hungarian railway lines with straight track portions. Calculations included through-rolled axle tons. (i.e., the track loading, MGT—million gross tons). The measurement data were "produced" by the FMK-007 track geometry measuring vehicle owned and operated by MÁV CRTI Ltd. (MÁV Central Rail and Track Inspection Ltd., Budapest, Hungary). Twenty-five cm track geometry was measured raw. Data analysis included mean, standard deviation, skewness, kurtosis, and Vaszary-type shape numbers of distribution functions. The eleven railway lines were also spectral analyzed. The track gauge change, average and standard deviation readings, elapsed time, and traffic loads did not correlate. (i.e., MGT). The gauge value distribution functions for the ten lines were neither Gaussian nor lognormal. Distribution functions are flatter at lower track speeds and steeper and narrower at higher speeds.

Fischer et al. [10] investigated the change in track gauges in curves for numerous railway lines in Hungary with low and heavy traffic (the same railway lines as in [12]). The curves included transition curves (TCs), circular curves (CCs), and entire curves. (ECs). The distribution functions were used to assess the change in the track gauge parameter as a function of elapsed time. The Kolmogorov–Smirnov test was used to conduct a statistical test, and the skewness and kurtosis parameters were computed and examined. The scientists determined that the kind of track system and sleeper type also had an impact on the change. The publication includes the precise deterioration ratios for every case study.

Track inspection train field data are used to analyze track geometry abnormalities' time-frequency characteristics [11]. The cumulative difference from the mean value is obtained using auto-adaptive signal decomposition on four pre-selected track sections. The sensitive wavelengths of track abnormalities are acquired from the suitable allocation of wavelength ranges in the Fourier Amplitude Spectrum (FAS) of the original signal and the Fourier transform of the components identified by the Variational Mode Decomposition (VMD). Track Quality Index (TQI) can detect track faults and right/left rail waveforms. The track gauge is broad-band, whereas the alignment parameter is narrow-band. The "manual" component separation and auto-adaptive component decomposition approaches were examined independently. Empirical mode decomposition's (EMD) original track gauge Intrinsic Mode Function (IMF) was non-stationary. Variational Mode Decomposition separated the clustered components within the IMF retrieved by EMD and the physically relevant trend of the parameters, producing equivalent results to FAS-based manual component separation. The extracted modes' spectral peaks are thought to come from track-vehicle mutual excitation and need vehicle dynamics calculations. This extra information regarding rail irregularity waveforms will help railway engineers identify early track stability issues and investigate track anomalies.

Aharkov et al. [32] examined the gauge stability of KB-75, KKP-1, and KPP-5 rail fasteners utilized in the Ukrainian railway network. Mathematical statistical ap-proaches compared railway track measurements. The study used 12 data sets from three-monthly assessments over three years. The study's straight line has 60 million MGT of mixed passenger and freight train traffic.

Ahac and Lakusic [33] modeled tramway gauge deterioration for maintenance planning. They created a theoretical-practical mechanistic-empirical deterioration model. They studied track gauge adjustments (primarily widening) on Zagreb's 1000 mm gauge tramway network. They examined Ri-60 "grooved rail" rail profiles and R200 and R260 rail grades for R > 200 m and R < 200 m site radii. Tracked and direct rail reinforcing were proposed. This study examined a 4.5 km portion of 25 Zagreb tramway segments constructed and rebuilt between 1997 and 2004. Track geometry (only straight sections were considered), traffic characteristics (only "open track" sections with separated track structure, no tram stops or level crossings, and a constant average speed of 15 km/h were considered), and rail quality and rail reinforcement were homogeneous.

Akkermann and Akkermann [34] addressed rail gauge trajectory and track micro- and macro-profile. In addition, they presented a track gauge parameter-monitoring digital clone in their article.

Falamarzi et al. [35] used an ANN (artificial neural network) and SVM (support vector regression) to forecast electrified track gauge variation. Each model's goodness of fit was determined using $R^2$ and MSE (mean squared error). The Melbourne light rail network was studied: it is a 250 km double-track segment with 25 lines. In 2013 and 2014, non-contact optical measuring equipment measured a 10 m string length. Yarra Trams supplied statistics. First, mathematical filters removed outliers and noise from measurement data. Both ANN and SVM techniques yielded excellent results, although the deterioration model based on the ANN method predicted straight track portions more accurately than curved track sections.

### *1.3. Novelty of the Current Paper*

Based on the above literature review, the authors dealt with analyzing the track gauge parameter, i.e., one of the most critical geometrical characteristics of railway tracks.

The authors conducted a research and development (R&D) project for MÁV Hungarian State Railways Ltd. on behalf of the Budapest University of Technology and Economics, Department of Highway and Railway Engineering. The project was entitled "Research and investigation of the causes of gauge narrowing by finite-element modeling in running track and turnout, and under operational and laboratory conditions" (see also the last paragraph of the Section 1.1). Using machine and manual track measurements, laboratory measurements, and theoretical considerations, the study's primary purpose was to investigate the causes of localized track gauge narrowing defects in railway tracks. The solutions proposed as a result of identifying the causes have the potential to reduce the frequency and severity of future local faults substantially. In addition, the study aimed to establish new concepts in less scientifically mature fields and provide techniques and instructions that expert engineers and practitioners can readily implement. The tight vehicle running is not the cause of the track gauge narrowing but a consequence, so it is not investigated in this paper.

## 2. Evaluation of the Track Gauge Data and Exploration of Possible Correlations between Error Points and the Superstructure System, Track Geometry, and Loading

### *2.1. Measurements with Measuring Cars*

The MÁV Central Track Inspection Ltd. (MÁV KFV Kft., Budapest, Hungary) performs track diagnostic measurements on the network operated by MÁV Zrt. (Hungarian State Railways Ltd., Budapest, Hungary) on the order of MÁV Zrt. two or three times a year. TEN-T (Trans-European Transport Network) lines are monitored with the FMK-007 measuring car and other lines with the FMK-004 measuring vehicle. The measuring car FMK-007 can measure at a speed of 200 km/h and is equipped with two measuring systems: a track geometry measuring system and a vehicle dynamic measuring system. The geometric measuring system provides distortion-free and contact-free data using optical and inertial measuring systems. The FMK-004 is a Plasser EM-120 self-propelled rail vehicle capable of measuring at 100 km/h. The measurement system is contact-based, i.e., the instruments on

the central bogie mounted on the vehicle and the measurement sensors mounted on the front and rear bogies by contact with the track. The measured raw data are stored at 0.25 m and evaluated as follows for both measuring cars:

- Track measurement graph showing the values of the measured characteristics by chainage;
- List of local geometric errors for the measured features;
- General track condition rating in the form of a rating number;
- Statistical evaluation.

The track measurement graph displays the geometric data on a graph similar to a long-section, which can be generated by loading the raw data into an office program and exported to PDF.

To be able to produce a list of local defects, it is necessary to have a set of dimensional limits against which the "defective" sections can be evaluated. MÁV Zrt. uses a multi-step size limit specification. For the purpose of this research, the measurement data and the size limits are required for the track gauge; the specifications of MÁV Zrt provide the size limit values. D.54, Chapter 51, is summarized in Table 1 [36]. The negative value of the track gauge (gauge narrowing) does not include a "D" category. Therefore, when assessing the gauge, not only local errors but also the moving average of the gauge values over 100 m shall be considered.

**Table 1.** Limit values of track gauge according to specifications of D.54 [36].

| **Speed** | **Gauge Widening [mm]** | | | | | | | **Gauge Narrowing [mm]** | | | | | |
|---|---|---|---|---|---|---|---|---|---|---|---|---|---|
| **[km/h]** | **A1** | **A2** | **B** | **C1** | **C2** | **C3** | **D** | **A1** | **A2** | **B** | **C1** | **C2** | **C3** |
| 0–80 | +5 | +10 | +15 | +25 | +30 | +35 | +45 | –4 | –4 | –5 | –7 | –8 | –9 |
| 81–120 | +5 | +10 | +13 | +20 | +25 | +30 | +45 | –4 | –4 | –5 | –7 | –8 | –9 |
| 121–160 | +4 | +7 | +11 | +15 | +20 | +25 | +45 | –4 | –4 | –5 | –6 | –7 | –8 |
| 161–200 | +3 | +5 | +9 | +10 | +15 | +20 | +45 | –3 | –3 | –4 | –5 | –6 | –7 |

The following tolerances are determined and detailed in [36].

A1 Construction limit: The gauge category whose limits shall not be exceeded by the geometric dimensions of a track constructed of new material (rail, sleeper, fastenings, new or renewed ballast in whole cross-section) on a new or renewed substructure.

A2 Construction limit: A gauge category whose limits shall not be exceeded by the geometric dimensions of the track constructed of used material (rail and/or sleeper not new and/or ballast not new or renewed).

B Maintenance limit: The gauge category whose limits shall not be exceeded by values achieved after maintenance works.

C1 action limit: Warning size limit category, which indicates the progressive deterioration of the track geometry. The evolution of the number of defects shall be monitored by comparing current and previous measurements.

C2 action limit: Intervention size limit category, which, if exceeded, requires maintenance work if the evaluation indicates that the local defect size is expected to reach the limit of C3 by the next track inspection measurement.

C3 action limit: Immediate action size threshold category, which requires action to be taken if reached: introduction of a speed restriction within a maximum of three days. After that, maintenance works of the track geometry must be carried out to remove the speed limit.

D closure limit: a limit category independent of the speed above which the track must be closed.

### *2.2. Evaluation of Local Gauge-Narrowing Errors*

The local gauge-narrowing data were available in Excel format based on measurements taken in the first half of 2015. In addition, the location data of the local faults were used to

determine the type of superstructure (in terms of the rail system and superstructure type) at a given location.

The local faults were plotted on a diagram using proprietary software, as shown in Figure 1. Stations and chainages were also displayed for easy location identification. The diagrams are mainly used to determine the number of defects and the distribution of defects. The height of the bars in the graphs is proportional to the value of defects, but values below the C1 size limit are not shown here as they are not considered measure size limits and are not included in the processed local error data set. It is, therefore, essential to emphasize that the dense columns indicate that the local values of gauge narrowing are densely above the local C1 error limit, but the sparsity of the columns does not mean that the gauge narrowing values on the given track section may not be close to the C1 size limit. As in Figure 1, the entire railway network has been evaluated for local gauge errors.

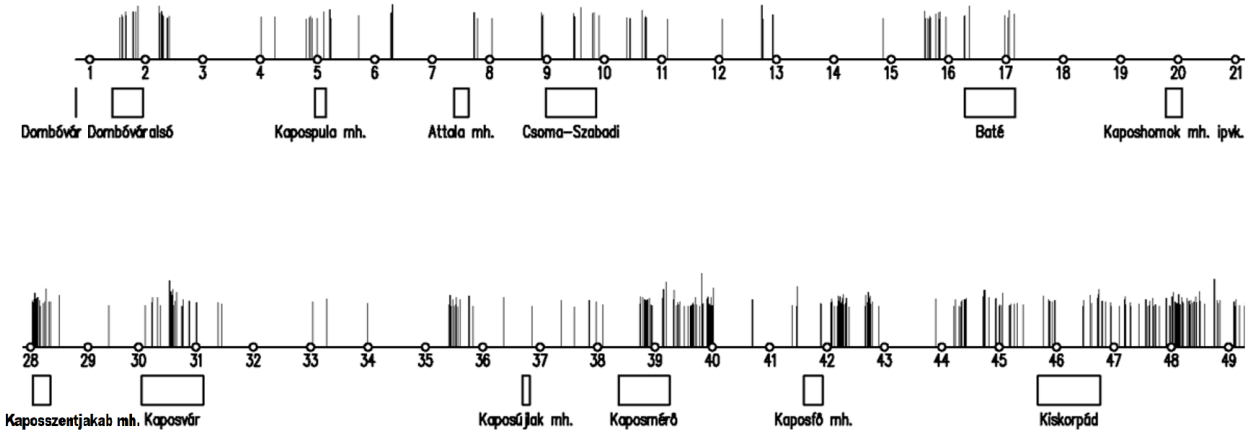



**Figure 1.** Example of diagram indicating local gauge-narrowing errors ("mh." means station stop, "ipvk." means siding connection).

### *2.3. Relationship between the Location of Track Sections with Gauge Narrowing and the Type of Superstructure*

The study was carried out on the TEN-T network using the results of the FMK-007 measuring car. The Hungarian railway network's most commonly used rail systems are MÁV 48.3, MÁV 48.5, 54E1, and 60E1. The study determined the total lengths of local defects by superstructure type based on the measurements of the MÁV track measuring car in the first half of 2015. The results show that even the railway lines with a rail system of 60 kg/m and almost exclusively with Skl-1 or Skl-14 tension clamp rail fastening only marginally reach the C1 gauge limit. It is due to the fact that these are the youngest sections on the national network.

Failures are more common in the tracks with 54 kg/m rails, but the frequency of mass occurrence is higher in the older 48 rail-system structures, which contain wooden inserts in the sleepers for the bolts of the fastenings.

Although the 54 rail superstructure also has a significant length of gauge narrowing, the length of tracks with this superstructure is also greater than that of the 48 kg/m system tracks. The results show that while 0.15% of the 54-system superstructure has at least C1 gauge narrowing, the same value for the 48.3 and 48.5 superstructures is between 0.79 and 1.34%, which is significant. Sections exceeding the C3 size limit are around 6% of the total length of sections exceeding the C1 size limit.

### *2.4. Relationship between the Location of Track Sections with Gauge Narrowing and the Alignment of the Track*

The correlation between local gauge errors and curvature was investigated for the TEN-T network using the results of the FMK-007 measuring vehicle. Table 2 shows the local errors of the straight and curved sections in percentage distribution. It can be seen that the gauge errors are concentrated in straight sections, with very few errors in curves.

**Table 2.** The relationship between curvature and gauge errors.

| Curvature of Track | Distribution of Local Errors in % | | |
|---|---|---|---|
| | **C1** | **C2** | **C3** |
| Straight | 95.5% | 94.5% | 93.3% |
| Curve | 4.5% | 5.5% | 6.7% |
| Sum | 100.0% | 100.0% | 100.0% |

### *2.5. Detailed Analysis of Selected Railway Lines*

For more in-depth studies, detailed raw data, measured at every 0.25 m, were also obtained for five main railway lines over several years, one of which is the 100a Budapest-Nyugati–Cegléd–Szolnok railway line. The analyses were carried out for the first half of 2010, 2013, and 2015 to identify the sections where track gauge C1 has not yet developed but is already present to some extent and the rate to which the gauge changes over time.

In the first step, the gauge values were plotted on a graph. The graph is similar to the track measurement graph but contains only the track gauge values in different colors, superimposed for the three years. According to the raw data format, the values are plotted with a deviation from the nominal 1435 mm.

The track measurement graph clearly shows the known correlations, such as the wear of the outer rails in the curved sections and its progression as a function of time. In addition, the sections with different gauge averages are distinguishable.

However, the different stages were not determined by visual inspection but by the so-called cumulative deviation from the mean method. The steps of the cumulative deviation from the mean method are as follows:

- Determine the average of the individual values of the track gauge (TG) of the line in the test ($\overline{x}_{TG}$):

$$\overline{x}_{TG} = \frac{\sum_{i=1}^{n} x_{TG,i}}{n} \tag{1}$$

- Calculation of the value of the cumulative deviation ($S_{TG}$) from the mean at a given measurement point '$i$': its value is the sum of the deviations from the mean of all points between point 1 and point $i$,

$$S_{TG,i} = \sum_{i=1}^{n} (x_{TG,i} - \overline{x}_{TG}) \tag{2}$$

- Display the values on a graph (Figure 2).

Different attributes have been assigned to the sections—such as stations, type of superstructure, and curvature—to help to identify the location and draw conclusions.

For five selected railway lines, the division into homogeneous sections and the time series averages for each section were analyzed line by line, and the conclusions were drawn.

### *2.6. Analysis of the 100a Budapest Nyugati-Cegléd-Szolnok Line, Right Track*

To analyze gauge variation, the curved and straight track sections have been separated. The remaining sections were classified as "mixed" sections, with several curves and intermediate straight lines.

For purely curved sections (or sections with several consecutive curves), the overall change in gauge over time is that there is no contraction in these sections, but the gauge increases due to the wear of the outer rail. Based on this, the rail's gauge expansion and wear rate were found to be 0.47–0.50 mm/year.

The variation of the gauge in straight sections with time is shown in Figure 3. Many longer straight sections were investigated along the entire line, 20 in total. These straight sections are shown in different colors, with the initial chainage of the straight section on

the legend. The rate of change of gauge is slightly variable for each section, based on the individual graphs, with the 2013 measurement showing an increase of 0.5–1 mm compared to the previous year, followed by a decrease of 0.5–1 mm in 2015. The regression line plotted on the mean of the values is marked with a bold red dashed line.

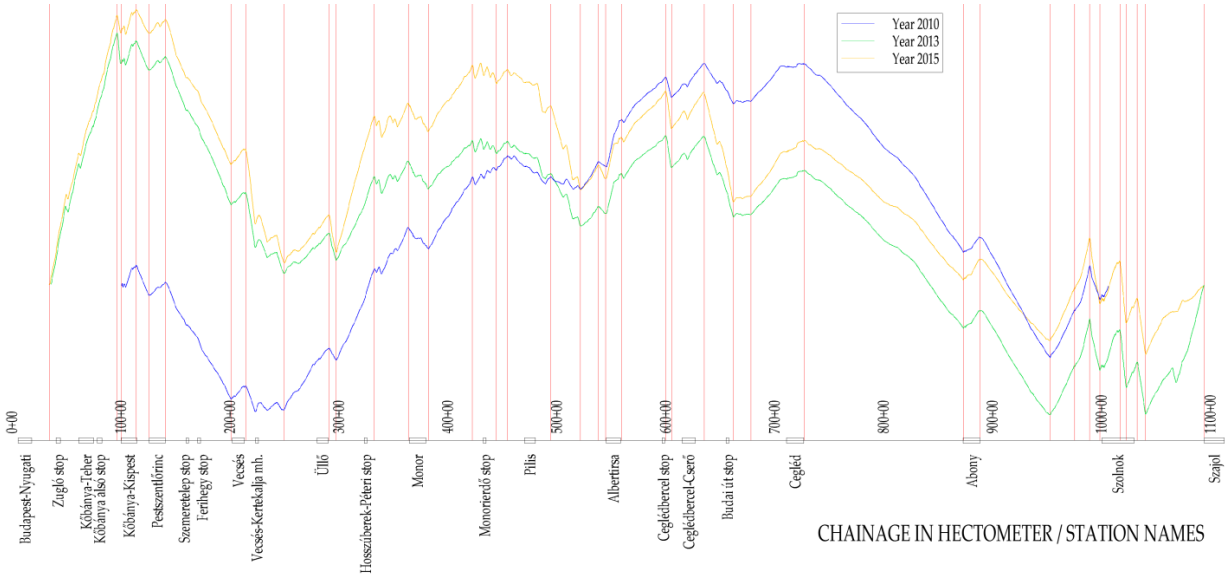



**Figure 2.** Example of dividing the track into sections by the cumulative deviation from the mean method (the red vertical lines illustrate the considered section borders for the calculation of cumulative deviation between Budapest-Nyugati and Szajol railway stations).

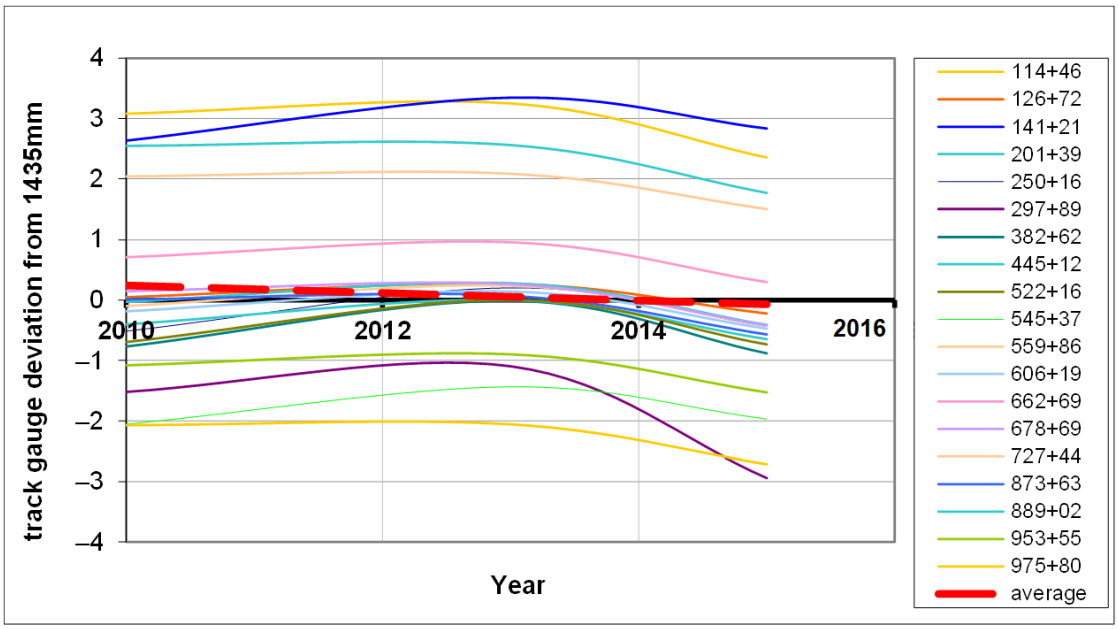



**Figure 3.** Change of gauge in straight sections of line 100a in the function of time.

The curves shown in the graph show a wide variation, possibly due to the track structures' different age, type, and conditions. It is, therefore, worth grouping the curves according to the superstructure system, as shown in Figure 4. Figure 4 shows that sections with 54 rail systems typically have a small gauge narrowing (1.0–2.5 mm), while sections with 60 systems tend to have a normal value or a small narrowing but with a considerable variation. The sections that differ in the "upstream" direction, i.e., in the direction of the widening, are the open line sections Kőbánya-Kispest–Vecsés and the Cegléd–Szolnok "A"

junction (both with 60E1 rail system). The difference is particularly striking between the latter open line section and the Abony through the track (60 rail), built simultaneously, where the gauge averages show a difference of 2 mm. It may be explained by the fact that the L2 sleepers were built with different dimensions so that a +2 mm gauge widening is included, while the "*LW-type*" sleepers were built with a 1435 mm gauge.

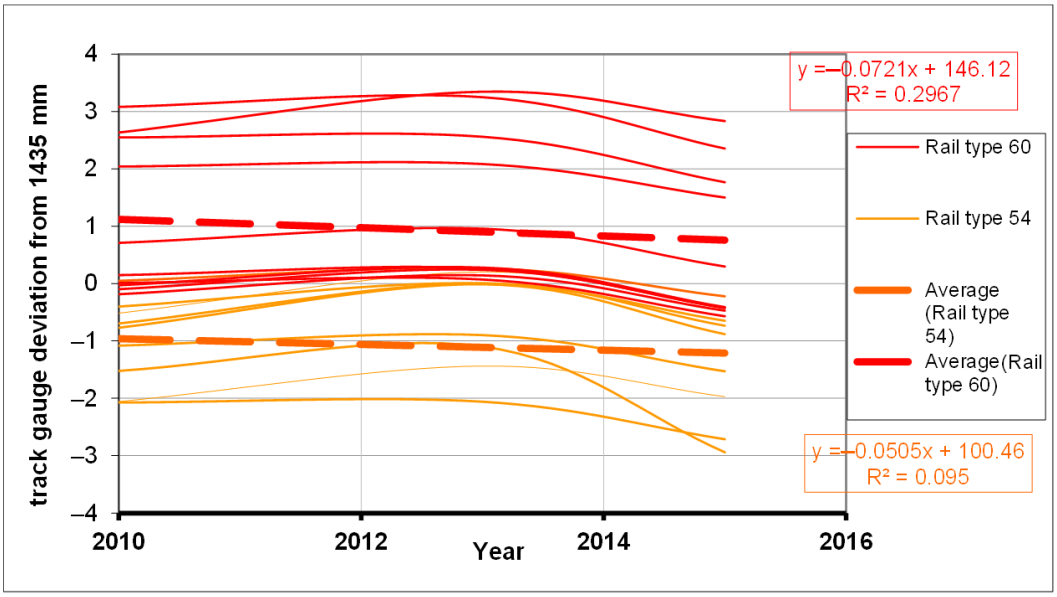



**Figure 4.** Change of gauge in straight sections of line 100a in the function of time (classified according to rail system).

### *2.7. Consequences of the Tests*

Based on the authors' analysis, it can be concluded that gauge narrowing is typical for straight sections; it is not generated in curved tracks. It is because the lateral force occurring in curved sections generally causes rail wear, compensating for a possible narrowing of the track and gaps due to the dimensional tolerances of the rail fastenings, which act in the direction of the gauge widening.

The average growth rate of the gauge widening on curved sections for all rail sections on the studied lines is ≈0.5 mm/year. On straight track sections, the gauge of the old 48 rail-system superstructures narrowed at 0.15–0.25 mm/year over time.

Regarding gauge narrowing, the MÁV48.5 rail-system superstructure is the most affected. The explanation is that these superstructures are old, 50–55-year-old structures are common on the main lines, and the aging processes are already increasing. In straight sections, the gauge narrows as time progresses. The most affected are the concrete sleepers originally constructed with wooden inserts marked "*T-type*" and "*L-type*" and for the MÁV48 rail system, where the wooden inserts' aging and the water ingress into the dowels initiate a serious deterioration process.

The straight track sections with the UIC54 and UIC60/60E1 rail system are younger and did not or only slightly increase gauge narrowing over time.

## 3. Investigation of Gauge in Operational Tracks and in Laboratories

The authors conducted a field survey of the railway tracks regarding track gauge and rail profile at 15 track locations. From the on-site measurements of the track gauge, rail web, railbase, and ribs of baseplates, it was concluded that the most significant contributor to the development of gauge narrowing is the improper positioning (loss of distance) of the baseplate. It may be due to corroded wooden inserts in the cross sleepers or damage to the plastic dowels, possibly due to the expansion of the holes in the baseplate. This observation was particularly true for the 48 kg/m rail-system superstructure ("*L-type*" cross sleepers).

Another but less significant cause of gauge narrowing is a change in the inclination of the rail. It was mainly observed in measuring the 54 and 60 kg/m rail-system superstructures but was insignificant in the 48 system. The change in rail inclination causes a maximum of 2 mm of gauge narrowing per rail by changing the rail inclination from 1:20 to approximately 1:16. More detailed measurements show that it is rare to see a marked increase in the cant of both rails.

The effect of increasing inclination of the rail was most evident in the 60 rail-system superstructure with direct flexible rail fastening, where the railpad under the rail was probably compressed asymmetrically, contributing to the development of gauge narrowing by 1-1 mm per each rail. However, it should be noted that such locations had the lowest effect on the total gauge narrowing of all the measured locations, which did not even reach the C1 warning limit.

The authors also carried out more measurements at three sites using instruments for the inclination of the rail and the rail profile itself. The site measurements confirmed the findings on rail inclination; the rail inclinations were not greater than 1:16, and a significant increase in inclination occurred in only one rail at a time.

Based on the field tests, 15 concrete sleepers were selected, removed from the track, and transported to the department's laboratory for more detailed testing. In the laboratory, the dimensions that influence the track gauge, such as the base lengths, distances between the ribs of the baseplates, and the inclination of the surface supporting the rail were measured.

At 100% of the "*L-type*" sleepers suitable for the MÁV48 rail system, originally with wooden inserts for the bolts, and at that time already 40–50 years old, it was observed that the baseplates could be moved by hand with an amplitude of about 5–7 mm due to the breaking of the double washers and the loosening of the bolts. This condition is unsuitable for ensuring gauge, and any gauge can develop. Theoretically, the movement could be as small as 1 mm (bore-to-screw diameter difference), but more significant movements may occur due to thinning of the screws due to corrosion and slight expansion of the holes. It is important to note that the rail bolt was adequately fixed in many cases, but the baseplate still moved on the sleeper due to the lack of clamping force. It is a conclusion that even with an intact dowel, the clamping effect is not always adequate, and this effect is difficult to detect in an assembled track.

## 4. Finite Element Modeling of Concrete Sleepers

### *4.1. Structure of the Model*

A finite element (FE) model of concrete sleepers has been assembled to investigate how the effects during the manufacture of concrete sleepers, their installation in the track, and during operation affect the development of gauge narrowing.

For various finite element software packages, the modeling possibilities of the design and check calculation of reinforced concrete sleepers were investigated. The triaxial (three-axis) behavior of concrete can only be formulated using a continuum model. Using the ANSYS program, a basic model describing the behavior of concrete sleepers was developed, which describes the spatial deformation and stress state of prestressed reinforced concrete sleepers more accurately than previous models.

The geometric and strength data of the reinforced concrete sleeper were calculated based on the "*L4 SV-type*" sleeper used on the Hungarian railway network (see Figure 5). The length of the sleeper is 2.60 m, its width is 300 mm on the bottom surface, the height under the rail is 215 mm, the weight is 326 kg, and the class of strength of the concrete is C50/60.

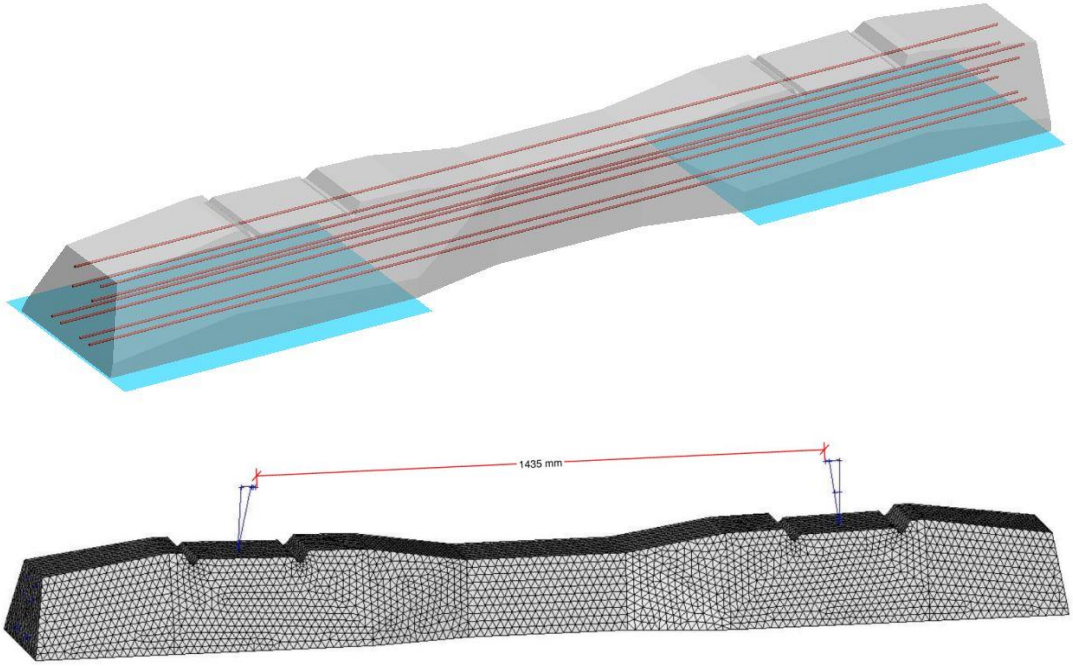



**Figure 5.** Schematic figures on the modeled *L4 SV-type* pre-tensioned reinforced concrete railway sleeper (above part: a 3D model with the steel tendons; below part: the applied mesh in the FE model).

The applied rail system is 60E1, its moment of inertia is $I = 30.55 \times 10^6$ mm$^4$. The inclination of the rail is 1:40.

Other relevant details of the FE model:

- The environmental categories of the concrete are XC4, XF3, and XA1 [37];
- There are eight pieces of steel tendons, type Y1770C-6.0-I, diameter 6.0 mm in accordance with [38];
- 69,000 body elements of the sleeper;
- 1000 rod elements (tendons);
- The sleeper was modeled by connecting the rail crown (top of the rail) finite element points in a rigid body (the height of the 60E1 rail profile is 172 mm; however, the rail gauge is measured 14 below the top of the rail and the rail inclination is 1:40, i.e., the height of the rigid body is $172 - 14 = 158$ mm as well as the width of the rail head at this height is 72 mm, i.e., the lateral dimension is $72/2 = 36$ mm; all these values are measured from the mid-point of the rail foot);
- The bolt holes for rail fastener screws were neglected;
- The initial tension of the steel tendons was 305 kN at the eight pieces; initial tensional stress is approximately 1350 MPa;
- The final stress value was considered with 1230 MPa;
- The final value of shrinkage $5.2 \times 10^{-4}$ m, i.e., 0.52 mm;
- The creep factor was taken into consideration with 1.85.

### *4.2. Loads and Supports*

For the vertical loads, an axle load of $Q = 250$ kN was assumed (it is the maximum axle load based on LM71 type vehicle load), equivalent to a wheel load of $Z = 125$ kN, and the speed was chosen to be $V = 160$ km/h (it is the maximum allowed speed in Hungary). Based on the principle of a longitudinal beam with continuous elastic bedding, the Zimmermann method was used with the Eisenmann dynamic factor to calculate the vertical load per sleeper. The sleeper spacing is $k = 600$ mm, and the surface of the half-sleeper on the ballast bed is $A = 850 \times 300$ mm$^2$, from which the width of the replacement longitudinal beam is $s = A/k = 425$ mm. The bedding factor can be $C = 0.05$ N/mm$^3$ for poor subsoil, $C = 0.10$ N/mm$^3$ for good subsoil, and $C = 0.11 - 0.15$ N/mm$^3$ for very good subsoil (all

values are from [39–41]). The harder subgrade is the standard for the force transmitted from the railbase to the sleeper, so the authors' calculations used a value of $C = 0.15$ N/mm$^3$.

According to Eisenmann, the dynamic multiplication factor ($\beta$) can be calculated as follows [39–41]:

$$\beta = 1 + t \cdot \alpha \cdot \varphi \tag{3}$$

where for a medium quality superstructure $\delta = 0.2$; for probability 0.997 $t = 3$ is assumed and $\varphi$ is the speed-dependent factor ($t$ must be 3.0 in the case of dimensioning) [39–41]:

$$\varphi = 1.0 + \frac{V - 60}{140} = 1.0 + \frac{160 - 60}{140} = 1.714 \tag{4}$$

The value of the dynamic factor [39–41]:

$$\beta = 1 + t \cdot \delta \cdot \varphi = 1.0 + 3 \cdot 0.2 \cdot 1.714 = 2.03 \tag{5}$$

The force $F$ transmitted to the sleeper from the rail according to the Zimmermann–Eisenmann function [39–41]:

$$F = \frac{k \cdot Z}{2 \cdot L_{lrb}} \cdot \beta \cdot \sum \eta \tag{6}$$

where $L_{lrb}$ is the length of the longitudinal replacement beam [39–41]:

$$L_{lrb} = \sqrt[4]{\frac{4 \cdot E \cdot I}{C \cdot s}} = \sqrt[4]{\frac{4 \cdot 2.15 \cdot 10^5 \cdot 30.55 \cdot 10^6}{0.15 \cdot 425}} = 801.2 \text{ mm} \tag{7}$$

The value of the influence line of deflection is $\eta = e^{-\xi}(\sin \xi + \cos \xi) = 1$, where $\xi = x_{dist}/L_{lrb}$, $x_{dist}$ is the absolute distance from the cross-section.

The load transmitted to the sleeper from the railbase [39–41]:

$$F = \frac{k \cdot Z}{2 \cdot L_{lrb}} \cdot \beta \cdot \sum \eta = \frac{600 \cdot 125}{2 \cdot 801.2} \cdot 2.03 \cdot 1 = 95.0 \text{ kN} \tag{8}$$

It should be noted that combining a medium-rated superstructure and a speed of 160 km/h is an extreme case; however, a very good subgrade was chosen as a boundary condition to maximize the force transmitted at the railbase. For this reason, the authors did not consider it appropriate to set the influence line of the deflection line to a value greater than 1.0 since this value will only be higher for locomotive bogies and only in exceptional cases for loaded trainsets.

The maximum value of horizontal lateral load ($Y_{max}$) based on previous experimental measurements [39–41]:

$$Y_{max} = 0.54 \cdot \left(10 + \frac{2}{3} \cdot Z\right) = 0.54 \cdot \left(10 + \frac{2}{3} \cdot 125\right) = 50.4 \text{ kN} \tag{9}$$

Of this load, approximately 65–70% is conveyed onto one sleeper ($Y_{max}^{sleeper}$)—it is because the results of load distribution based on the Zimmermann-calculation method in the worst case (see [39–41]):

$$Y_{max}^{sleeper} = 0.65 \ldots 0.70 \cdot Y_{max} = 33 \ldots 35 \text{ kN} \tag{10}$$

Based on the above, the forces from the wheel loads of the vehicles acting on a rail support surface of the sleeper are calculated to be 95 kN vertically and 35 kN horizontally with the point of application of the horizontal force 14 mm below the railtop level.

In the modeling of concrete sleepers, two types of load transfer were investigated: one is centric, and the other is eccentric. In the case of concentrated loading, the sleepers and the ballast are adequately supported and maintained, with a half-sleeper bearing surface of $A = 850 \times 300$ mm$^2$ on the ballast bed (Figure 6). In Figures 6 and 7, the red pyramid is an

infinite rigid mesh, which means the uniform distribution of the concentrated force on the surface on the bearing surface under the rail in the FEM model.

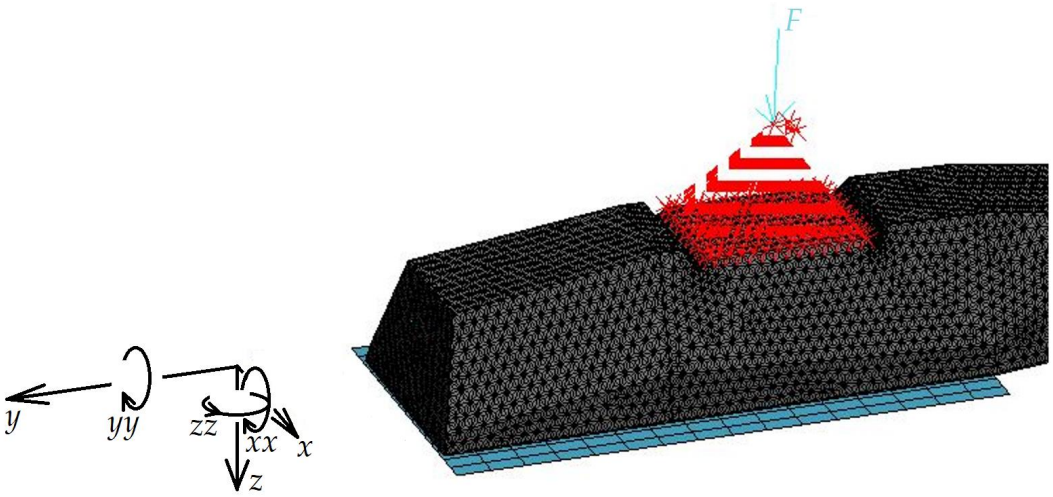



**Figure 6.** Central loads and supports in normal operation (the red–white tetrahedron symbolizes the load distribution from the rail head to rail foot to be able to consider realistic loading onto the modeled sleeper). Below the sleeper, a surface was considered to support the sleeper; see the meshed "plate".

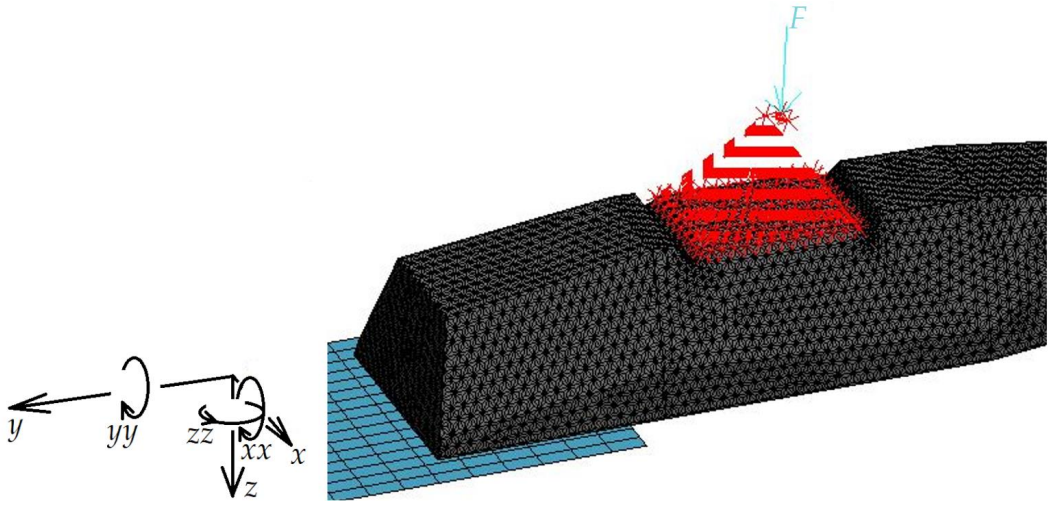



**Figure 7.** Eccentric loads and supports (the red–white tetrahedron symbolizes the load distribution from the rail head to rail foot to be able to consider realistic loading onto the modeled sleeper). Below the sleeper, a surface was considered to support the sleeper; see the meshed "plate".

However, the effect of uneven support of the sleepers (uneven tamping, tamping only the part of the sleeper outside the rail, water bag, etc.) on the deflection of the track was also investigated. The case was modeled where the wheel load is not transmitted uniformly from the sleeper to the ballast but eccentrically, and the sleeper is supported on the ballast for only 300 mm long from the ends of the sleepers due to uneven tamping or highly inhomogeneous loadbearing of the substructure (Figure 6). In the case of eccentric loading, the point of application of the vertical load is in the third of the railbase towards the centreline of the track, and the sleepers are supported only over a length of 300 mm from the end of the sleeper, with a support area of 300 × 300 mm. The central and eccentric support models are illustrated in Figures 6 and 7.

In the modeling, the effects of concrete shrinkage, creep, and relaxation of the prestressing wires were also taken into account.

*4.3. Cases of Assessment*

The tests should be analyzed from the perspective of the amount of gauge narrowing caused by changes in displacement boundary condition (support) and by loads, taking into account rheological changes. In all cases, the initial gauge was 1435 mm, and the modeling was carried out relative to this. The following cases were investigated:

(a) 50 days; relaxation, creep, shrinkage;
(b) 100 days; relaxation, creep, shrinkage;
(c) 400 days; relaxation, creep, shrinkage;
(d) Same as (c) + operational central loads;
(e) Same as (c) + operational eccentric loads;
(f) Same as (e) + 35 °C cooling of temperature;
(g) Same as (e) + 10% over-tensioning of the wires;
(h) 400 days; eccentric loads, self-weight.

There are further details for the above cases. The tests should be viewed from the perspective of the amount of compression caused by changes in displacement boundary condition (support) and force, taking into account rheological changes. The age of the concrete sleeper is also given when considering the rheological effects.

In these investigations, it was assumed that the rails are placed on the concrete sleepers at 50 or 100 days of age, at which time the railway track geometry is adjusted; i.e., it will take around 50–100 days from production to installation. During this time, the sleepers will have a length change caused by tension, relaxation, creep, and shrinkage. These are the baseline data, i.e., the so-called "zero" values regarding pressure shrinkage. Here, they are controlled (adjusted), and the railway can run without any rail gauge narrowing. Over time, however, the sleepers suffer further length changes, which are corrected only by repeatedly correcting the pressure contraction determined by the mandatory periodic inspections. This date was taken in the current study to be the 400th day after the manufacture of the sleepers.

Based on the above-mentioned facts, the shrinkage of the concrete was taken into account in all cases (see Figures 8 and 9) when determining our calculation cases, and the same accounting was performed for relaxation and creep.

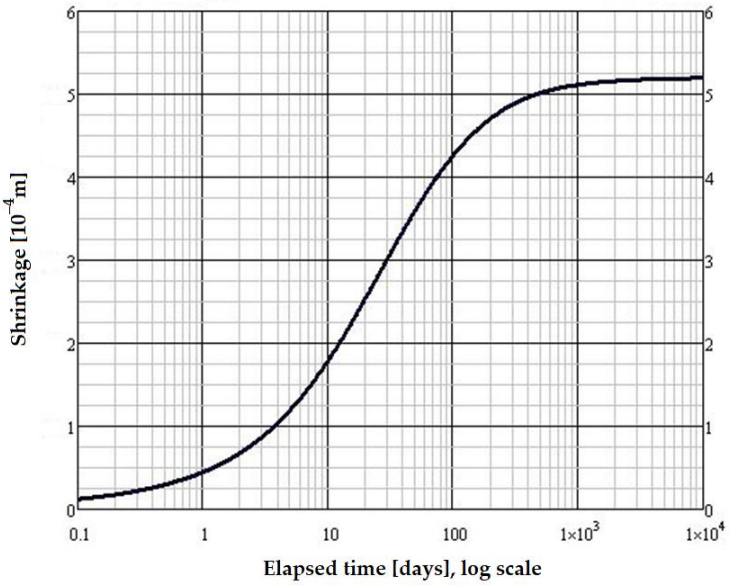



**Figure 8.** Calculated shrinkage of the concrete until the first 10,000 days after manufacture.

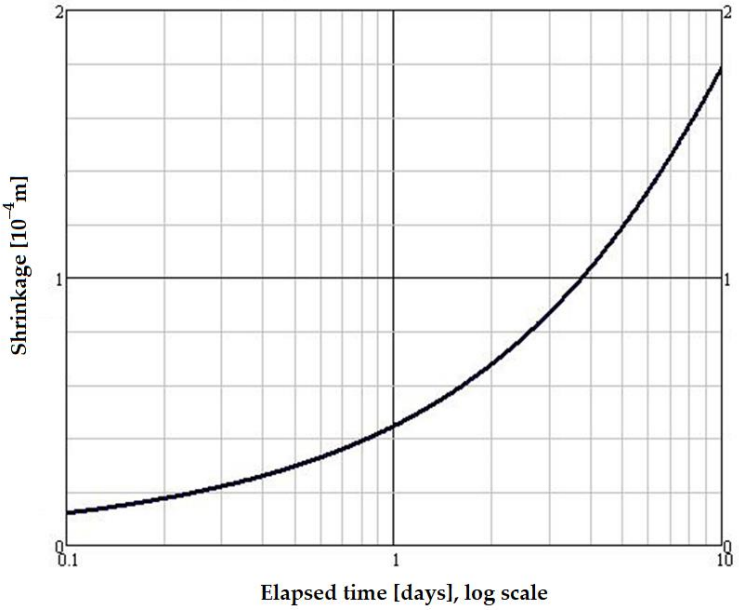



**Figure 9.** Calculated shrinkage of the concrete until the first ten days after manufacture.

The method used to determine the creep rate is based on Section 3.1.4 of EN 1992-1-1 [42]. Assuming an outdoor environment, 0 days of prestressing, and the designed concrete strength class, the creep factor was found to be 1.85. Consequently, the long-term modulus of elasticity of the concrete will be equivalent to a value of (1 + 1.85). The actual concrete structure (real concrete mix) has a much higher strength. It only reduces the creep, so our estimate will be upper bound.

The relaxation of the prestressing wire was calculated according to Section 3.3.2 of the literature [42], assuming a stress loss of 2.5% at 1000 h. The manufacturer provides this latter value, but it is the guaranteed value for modern reduced relaxation wires (tendons) used today. Note, however, that this value could be as high as 8% for old conventional relaxation wires.

### *4.4. Results*

Figure 10 illustrates the results of case (a). Due to the limited space, the authors decided not to publish all the details with similar figures related to FE modeling.

Table 3 summarizes the results of the computer runs (parametric tests). The cases represent the combination of effects considered. The gauges and the value of the narrowing are given separately.

**Table 3.** Values of gauge narrowing.

| Load Case (See Section 4.3) | Description of Load Case | Gauge [mm] | Narrowing of Gauge [mm] |
|---|---|---|---|
| (a) | 50 days; relaxation, creep, shrinkage | 1434.39 | 0.61 |
| (b) | 100 days; relaxation, creep, shrinkage | 1434.24 | 0.76 |
| (c) | 400 days; relaxation, creep, shrinkage | 1434.00 | 1.00 |
| (d) | Same as *c*; +operational central loads | 1433.95 | 1.05 |
| (e) | Same as *c*; +operational eccentric loads | 1427.00 | 8.00 |
| (f) | Same as *e*; +35 °C cooling of temperature | 1426.62 | 8.38 |
| (g) | Same as *e*; +10% over tensioning of the wires | 1426.46 | 8.54 |
| (h) | 400 days; eccentric loads, self-weight | 1433.78 | 1.22 |

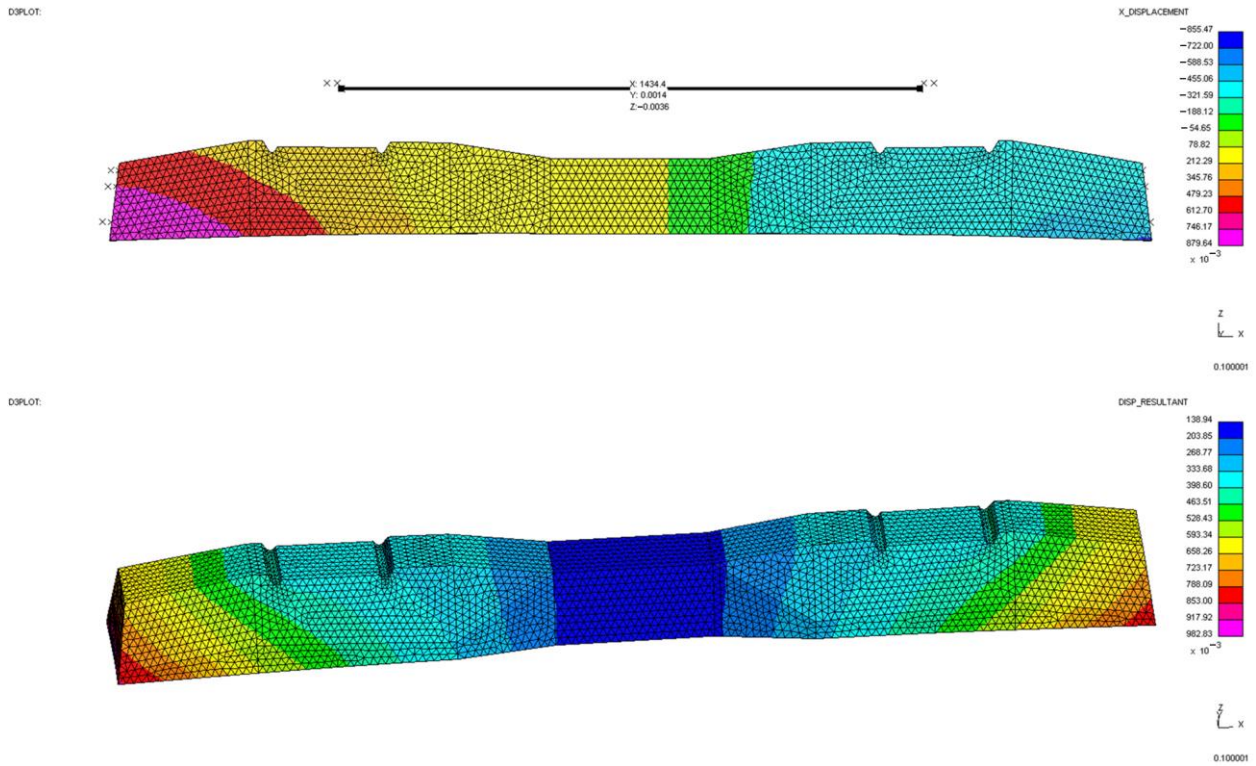



**Figure 10.** The *x-direction* (**above part**) and total displacement (**below part**) plots, in the case of (a), are based on Section 4.3. The legend shows values with $10^{-3}$ mm units.

The calculations were based on the assumption that after the sleepers are manufactured, they are stored at the manufacturer's site, then transported, possibly also stored before installation, then installed, the rails are placed, and their track gauge is adjusted. From production to the track alignment takes about 50–100 days. During this time, the sleepers will have a length variation caused by tension, relaxation, creep, and shrinkage. These values are shown in rows '(a)' and '(b)' of Table 3. These are the initial baseline data, i.e., the "0" (zero) values for the gauge narrowing. It is because the track and gauge are controlled here, and the railway can run without narrowing. Over time, however, the sleeper suffers further length variations, determined by the mandatory periodic inspections and corrected only by repeated maintenance works. Therefore, this date was taken in the authors' tests to be the 400th day after manufacture.

At 50 days of age, the gauge narrowing (row "a" in Table 3) is 0.61 mm. This value can also be taken as a baseline, the "0" (zero) value. At 100 days of age, the gauge narrowing (row 'b') is 0.76 mm, which can, of course, also be taken as a baseline if someone assumes that the rail positioning and gauge is set on this day; i.e., this value can also be taken as '0' for the gauge narrowing. The track gauge can be calculated from case 'a' or 'b' for the first time because this is the first time the track gauge is adjusted during construction works, and there is no narrowing at this time; the track gauge is still 1435 mm.

At 400 days of age, the gauge narrowing from production (Table 3, line "c") is 1.00 mm. Therefore, the gauge narrowing determined by the mandatory periodic supervision tests is assumed to be corrected by realigning at about 400 days from manufacture. In other words, if someone is looking for the value of the gauge narrowing between the 50th and the 400th day, a value of

$$N(a) = c - a = 1.00 - 0.61 = 0.39 \text{ mm} \quad (11)$$

is received, and if someone looks for the value of the gauge narrowing between day 100 and day 400, then a value of

$$N(b) = c - b = 1.00 - 0.76 = 0.24 \text{ mm} \quad (12)$$

is received.

These values are, of course, derived only from the sleepers' deformations without the trains' loads.

The load combination 'd' in the table shows the displacement results calculated from numerical modeling of the combination of relaxation, creep, shrinkage, and the in-service load for 400 days, with central wheel loads and central support on the ballast. In this case, the gauge narrowing of the sleeper was 1.05 mm from the date of manufacture. If the narrowing is calculated from the age of 50th or 100th days, the former values are as follows:

$$N(d - 50) = d - a = 1.05 - 0.61 = 0.44 \text{ mm} \quad (13)$$

or

$$N(d - 100) = d - b = 1.05 - 0.76 = 0.29 \text{ mm} \quad (14)$$

Significantly higher values are obtained if eccentric wheel loads are considered, i.e., if the support of the sleeper is only about 30–30 cm long at both ends and the vertical loads are also eccentric. In this case, the rate of gauge narrowing is 8.00 mm from the 0 date of manufacture, and considering it from the 50th or 100th day after manufacture, it is

$$N(e - 50) = e - a = 8.00 - 0.61 = 7.39 \text{ mm} \quad (15)$$

or

$$N(e - 100) = e - b = 8.00 - 0.76 = 7.24 \text{ mm} \quad (16)$$

These values are very significant compared to the normal case "d". They do not occur in the case of normal maintenance of the track and ballast but only in the case of extreme tamping and ballast deficiencies. It clearly highlights the need for professional track maintenance.

If, in addition to the effects of relaxation, creep, shrinkage, and the combination of external loads calculated for 400 days, a 35 °C cooling is included, the former values increase by a further 0.38 mm.

For an overstressing of the tension wires by 10%, the additional increase in gauge narrowing is 0.54 mm compared to case "e".

### *4.5. Conclusions*

Finite element modeling has shown that the sleeper's shrinkage and other time-dependent deformation do not contribute significantly to the development of the gauge narrowing. The maximum magnitude of the time-dependent effects remains below 1.0 mm. With time-dependent effects, central transfer of wheel loads, and proper support of the cross sleepers—careful maintenance—the cumulative rate of gauge narrowing is also around or below 1 mm, i.e., insignificant.

However, the uneven support of the cross sleepers and the eccentric transfer of wheel loads to the sleeper can cause a gauge narrowing of up to 7.39 mm. The cumulative values of these effects can lead to significant gauge narrowing of 8–9 mm. With careful design and maintenance, high narrowing values can be avoided by ensuring adequate and uniform support of the concrete sleepers. The results are summarized in Figure 11.

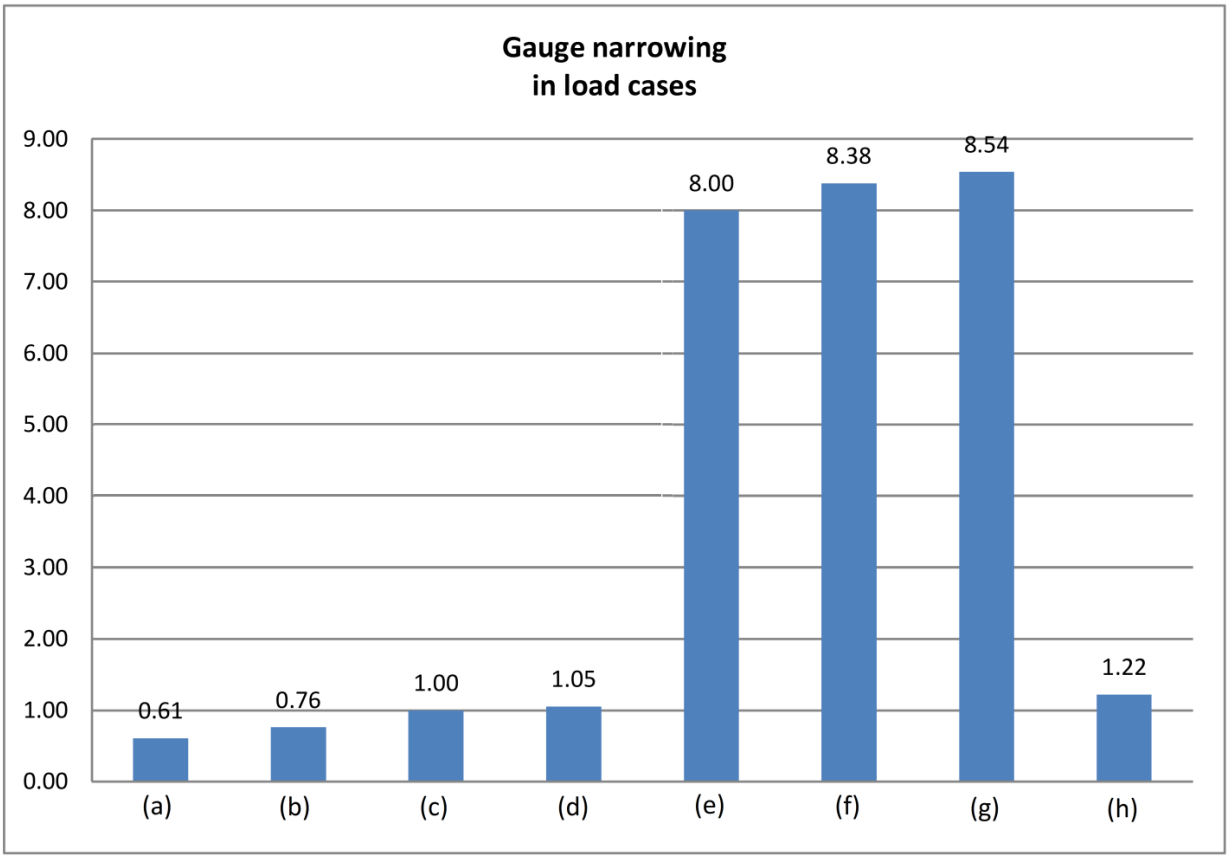



**Figure 11.** Result of gauge narrowing (all units are in mm) in the different load conditions (the legend from (a) to (h) are in accordance with Section 4.3).

## 5. Modeling of Lateral Stability of Rails under Loss of Function of Rail Fastenings

In this R&D work, the authors are trying to find answers to the question of what factors influence and what causes lead to the formation of a gauge narrowing. Taking into account the rail–wheel interaction, the following forces act on the rail:

- Vertical forces resulting from the static and dynamic wheel loads of the vehicles;
- Horizontal lateral forces from the irregular movements of the vehicles and non-compensated lateral accelerations;
- Longitudinal forces from breaking and accelerations of the vehicles and the temperature change in case of constrained heat expansion.

The track gauge is most affected by the lateral force, but it acts outward from the track axis, which also explains the phenomenon of wear on the leading edge of the rail. The present study shows that in curves, there is never a contraction of the gauge, but rather a widening of the gauge, which, depending on the radius of the curve, increases at a rate of 0.5–1 mm/year. However, a small or large degree of gauge narrowing occurs on straight track sections, especially on old, aged track sections.

Rail fastenings limit the movement of the rail normally in all six degrees of freedom on the sleeper (see Figures 6 and 7):

- Longitudinal rail restraint in the *x-direction*;
- Lateral support of rail in the *y-direction* and keeping the gauge;
- Vertical support of the rail in the *z-direction*, that is, to bear wheel loads;
- Restrict rotation in the *xx-direction* by two rail clips equally holding down the rail;
- Restrict rotation in the *yy-direction*;
- Restrict rotation in the *zz-direction*, that is, the torsional stiffness of the fastening to serve for the stability of the track against buckling.

Of the effects listed above, the variation in gauge is primarily caused by insufficient support in the *y-direction*. However, twisting in the *xx-direction* can also cause a gauge error since the railbase is supported, and the gauge is measured at the rail head. A change in the height of the railbase on either side also causes a displacement of the rail head.

The rotation in the *zz-direction* will cause a *y-directional* shift in the adjacent rail supports.

### *5.1. Thermal Forces in Case of Constrained Heat Expansion*

In a continuously welded rail track (CWR track), the following normal force is generated if the temperature of the track is not equal to the actual neutral temperature [39–41]:

$$N = \alpha \cdot E \cdot A \cdot \Delta T \tag{17}$$

For example, the compressive force developed in the 54E1 and 60E1 rails for temperature increases of $\Delta T$ = 45 and 50 °C, respectively, are given in Table 4.

**Table 4.** Compression force in the 54E1 and 60E1 rails due to an increase of temperature of 45 °C and 50 °C.

| **Increase of Temperature $\Delta T$ [°C]** | **Compression Force $F$ [kN]** | |
|---|---|---|
| | **54E1 Rail** | **60E1 Rail** |
| 45 | 776.28 | 853.38 |
| 50 | 862.53 | 948.20 |

In the case of standard track design, the actual neutral temperature at the time of construction should be set between +15 and +28 °C (neutral temperature zone) according to the Instruction of D.12/H "Instruction for the Construction, Maintenance and Supervision of CWR Tracks" of MÁV Zrt. [43]. Of course, the neutral temperature in the track can vary from place to place and is constantly affected by the displacement of the sleepers and longitudinal forces (e.g., by acceleration or braking of the trains or inhomogeneous ballast conditions, etc.). Maintenance works in the track (repair of rail fracture, replacement of a section of rail, turnout replacement, etc.) can all change the original neutral temperature. At certain time intervals, it may be necessary to release the tensile stresses in the rail and establish a new effective neutral temperature on a more extended section.

### *5.2. The Euler Force*

From the point of view of buckling, the compressive force at high temperatures is of interest. The minimum critical force $F_{cr}$ at which the rail loses its stability without lateral support should be investigated for the above reasons. According to Euler's theory of stability, the critical force $F_{cr}$ is the force at which the rail is in a state of equilibrium even in the deflected shape [39,40]:

$$F_{cr} = \frac{\pi^2 \cdot E \cdot I_y}{\lambda^2 \cdot l_{ws}^2} \tag{18}$$

In the present case, both ends of the rail are assumed to be fully fixed, i.e., $\lambda$ = 0.5. The computational results are summarized in Table 5 under the following assumptions:

- 1…16 rail fastenings do not have sufficient lateral support for the rail; beyond them, all fastenings are satisfactory;
- The cross-section of the rail cannot take a force greater than the force calculated from the yield strength and the cross-section of the rail, so the values in the table include not only the values calculated from the above formula but also the values calculated from the yield strength $\sigma_f$ = 500 MPa. These values are highlighted in red.

- The critical force $F_{cr}$ is greater than the thermal force in the rail in the range of smaller deflection lengths, so the rail remains stable under the maximum thermal compression force for deflection even if nine fastenings do not work laterally for 54E1 rails and 10 for 60E1 rails. The force $F_{cr}$ calculated, in this way, cannot develop in the rail due to temperature changes. These values are highlighted in yellow in the table.

**Table 5.** The critical force $F_{cr}$ belonging to different rail sections and unsupported lengths of rail.

| Number of Rail Fastenings That Have Failed $n$ [—] | Length of Rail without Lateral Support $l_{ws}$ [mm] | Critical Force $F_{cr}$ [kN] | |
|---|---|---|---|
| | | 54E1 | 60E1 |
| 1 | 1200 | 3488.50 | 3835.00 |
| 2 | 1800 | 3488.50 | 3835.00 |
| 3 | 2400 | 3488.50 | 3835.00 |
| 4 | 3000 | 3488.50 | 3835.00 |
| 5 | 3600 | 2745.46 | 3355.19 |
| 6 | 4200 | 2017.07 | 2465.04 |
| 7 | 4800 | 1544.32 | 1887.30 |
| 8 | 5400 | 1220.20 | 1491.20 |
| 9 | 6000 | 988.36 | 1207.87 |
| 10 | 6600 | 816.83 | 998.24 |
| 11 | 7200 | 686.36 | 838.80 |
| 12 | 7800 | 584.83 | 714.72 |
| 13 | 8400 | 504.27 | 616.26 |
| 14 | 9000 | 439.27 | 536.83 |
| 15 | 9600 | 386.08 | 471.82 |
| 16 | 10,200 | 341.99 | 417.95 |

If 10 fastenings fail for 54E1 rails and 11 fastenings fail for 60E1 rails laterally, the force generated in the rail by the temperature rise exceeds the critical compressive force for buckling, and the rail is not stable.

### *5.3. Investigation of Rail Length Variation as a Function of Initial Misalignment*

At temperatures higher than the actual neutral temperature, the compressive force in the rail is generated due to the inhibited length change. It also follows that if the length change is allowed, the compressive stress will decrease. Therefore, it is also necessary to consider whether the length change of the rail due to initial misalignment represents an amount of length change associated with a degradation of the stress. From the calculations, it is clear that in the case of a type A failure mode for different wavelengths and amplitudes, the change in length of the rail is negligible for amplitude values of initial misalignments. The change in length of rail due to the wavelength-amplitude pairs that can be formed is only 0.01–0.02 mm, which does not affect the thermal force and is only a few thousandths of the compression due to the thermal force.

### *5.4. Investigation of Rail Length Variation as a Function of Initial Misalignment*

It can be seen that in some cases—in case of inadequate lateral support of 9–11 fastenings—the rail may suffer lateral buckling. Therefore, examining the relationship between the longitudinal compressive force and the buckling is necessary. The theoretical straight rail is not applicable for such an analysis because the laws of mechanics state that the rail is in equilibrium, and only the critical force $F_{cr}$, which is associated with the loss of stability, as stated earlier, can be determined. The deflected shape cannot be determined.

The test is therefore carried out by assuming a distorted geometry of the rail, which can be modeled by a slight initial misalignment with an amplitude of $f$ and with a length of $l_{dist}$ and a type $A$. The shape of the wave is a half-cosine wave. Based on this, the function of initial geometrical distortion, in the function of $x$, is [39,40]

$$y_k(x) = \frac{y_{k,max}}{2}\left(1 - \cos\left(\frac{2\cdot\pi}{l_{dist}}x\right)\right) \tag{19}$$

The longitudinal force causes a bending moment in the structure, given that the shape of the beam is not straight. The magnitude of the bending moment as a function of $x$ [39,40] is

$$M(x) = F_{comp}\cdot y_k(x) = F_{comp}\cdot y_{k,max}\left(\cos\frac{2\cdot\pi}{l_{dist}}x\right) \tag{20}$$

According to the differential equation of the elastic beam, the applied bending moment is proportional to the curvature of the support, which is related to the following [39,40]:

$$\frac{1}{\rho(x)} = \frac{M(x)}{E\cdot I_y} \tag{21}$$

Based on the differential equation of the elastic beam, the curvature of the support can be used to determine the deflected shape of the beam as follows [39,40]:

$$\tau(x) = \int_0^x \frac{M(x)}{E\cdot I_y}dx \tag{22}$$

$$y(x) = \int_0^x \tau(x)dx \tag{23}$$

After the integrations and substituting $x = l/2$ [39,40],

$$y(x) = \frac{F\cdot y_{k,max}}{2\cdot E\cdot I_y}\cdot\frac{{l_{dist}}^2}{4\cdot\pi^2}\left(1 - \cos\left(\frac{\pi}{l_{dist}}x\right)\right) \tag{24}$$

The maximum of $y(x)$ occurs when the bracketed value is maximum. It occurs when $\cos\left(\frac{\pi}{l}x\right) = -1$, i.e., $x = l/2$. The function, therefore, reaches its maximum at half of the error length considered [39,40]:

$$y_{max} = \frac{F\cdot y_{k,max}}{E\cdot I_y}\frac{l_{dist}^2}{4\cdot\pi^2} \tag{25}$$

By substituting actual values into the formula, it can be seen that $y_{max}$ is greater than $y_{k,max}$, so the beam will bend due to the bending moment from the initial distortion but will consequently experience an even more significant bending moment, causing it to bend further. The equilibrium position is reached when the bending moment from the deflected shape is in equilibrium with the geometry of the deflected shape, i.e., [39,40]

$$y_{max} = \frac{F\cdot(y_{k,max} + y_{max})}{E\cdot I_y}\frac{{l_{dist}}^2}{4\cdot\pi^2} \tag{26}$$

In the above equation, it is assumed that the initial deflection $y_{k,max}$ does not include the bending moment in the rail; otherwise, the problem can be reduced to the case of a straight, free-of-distortion girder, and the actual deflection $y_{max}$ associated with the longitudinal force cannot be determined.

The $y_{max}$ deflection can also be determined by iteration. The maximum deflection $y_{max}$, derived from the bending moment $M(x)$ associated with the initial deflection $y_{k,max}$, is substituted back into the initial deflection value by increasing it by the original initial deflection $y_{k,max}$.

### 5.5. Analysis of the Force Greater Than the Critical Force in Case of Partial Lateral Support

The rail is held down by the rail fastenings in the *x*-, *y*- and *z-directions*; the standard sleeper spacing on main lines is 0.60 m. Based on the authors' field and laboratory tests, the experience is that the baseplates of the rail fastenings move laterally so that the lateral support of the rail is incomplete within certain limits. After an initial *y-directional* displacement, the baseplates are supported, but until then, their movement is possible within certain limits.

As shown in the previous chapters, if the compressive force exceeds the critical force $F_{cr}$, the track loses its stability without lateral support. However, as the baseplates, which are not provided sufficient lateral support, can only move freely up to a certain extent and then hit the rail bolt, lateral support can be provided but with a narrower track gauge. Thus, another equilibrium condition can be created, which, assuming a straight track, cannot be changed by the *z-direction* load of the railway vehicle.

At this point, the deflected shape will no longer be a pure sine curve because the lateral support of the rail may disturb it.

The support in the 9 m long model (with 16 fastenings) is assumed to be at the two middle sleepers ($k$ = 0.60 m sleeper spacing), each with a force $F_H$ (to achieve symmetry), as shown in Figure 12. The bending moment due to the supporting forces on the support is indicated by the green line in Figure 13. There are also bending moments at both fixed ends of the rail, the magnitude of which can be calculated from the boundary conditions.

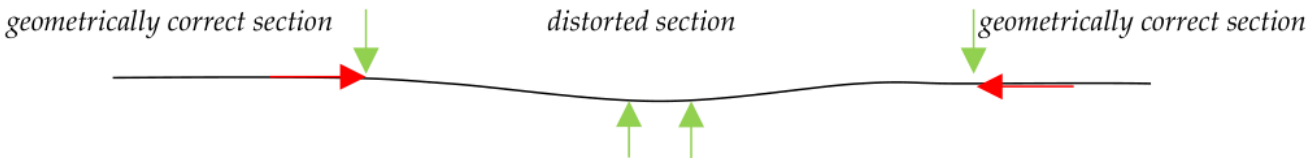



**Figure 12.** Forces acting on the rail with initial distortions ($l_{dist}$ = 9 m, 54E1; the horizontal arrows symbolize the longitudinal forces in the track; hence, the vertical arrows mean the transversal forces).

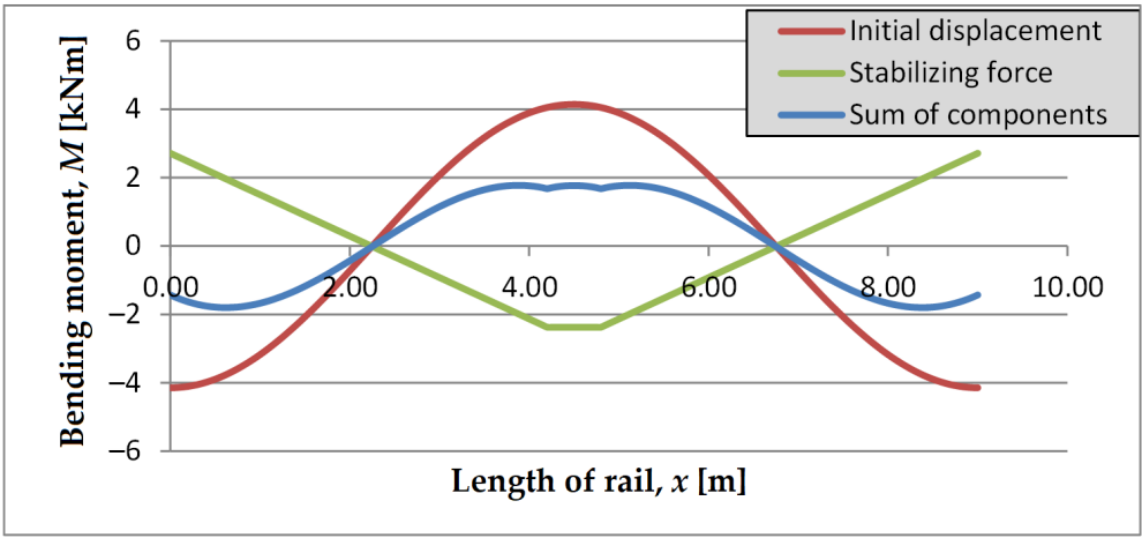



**Figure 13.** Bending moment in the rail with initial distortions ($l$ = 9 m, 54E1).

The differential equation of the elastic beam is [39,40]:

$$\frac{1}{\rho(x)} = \frac{M(x)}{E \cdot I_y} \tag{27}$$

The angle of the tangent of the rail at the length of $x$ [39,40]:

$$\tau(x) = \int_0^x \frac{M(x)}{E \cdot I_y} dx \tag{28}$$

Since both ends of the rail are fully fixed, they cannot rotate; therefore, $\tau(0) = 0$ and $\tau(l) = 0$ [39,40]:

$$\tau(l) = \int_0^l \frac{M(x)}{E \cdot I_y} dx = \frac{(l_{ws} + k) \cdot (l_{ws} - k) \cdot F_H}{2 \cdot E \cdot I_y} - \frac{M_F \cdot l_{ws}}{E \cdot I_y} = 0 \tag{29}$$

Consequently, the value of the bending moment at the two fixed ends of the rail [39,40] is

$$M = \frac{(l_{ws} + k) \cdot (l_{ws} - k) \cdot F_H}{4 \cdot l_{ws}} = 2.24 \cdot F_H \tag{30}$$

The authors are investigating the value of the force $F_H$ that can stabilize the track to a specified deflection value for a given initial deflection and a given longitudinal force. Since the track section is assumed to be symmetric, the lateral displacement will be the largest in the middle cross-section. Furthermore, an iterative numerical solution to the problem has been obtained since the function of the bending moment from the stabilizing force $F_H$ consists of several sections.

First, the function is determined by numerical integration, and from this—also by numerical integration—the lateral displacement function $y(x)$. An example of the displacement function is shown in Figure 14.

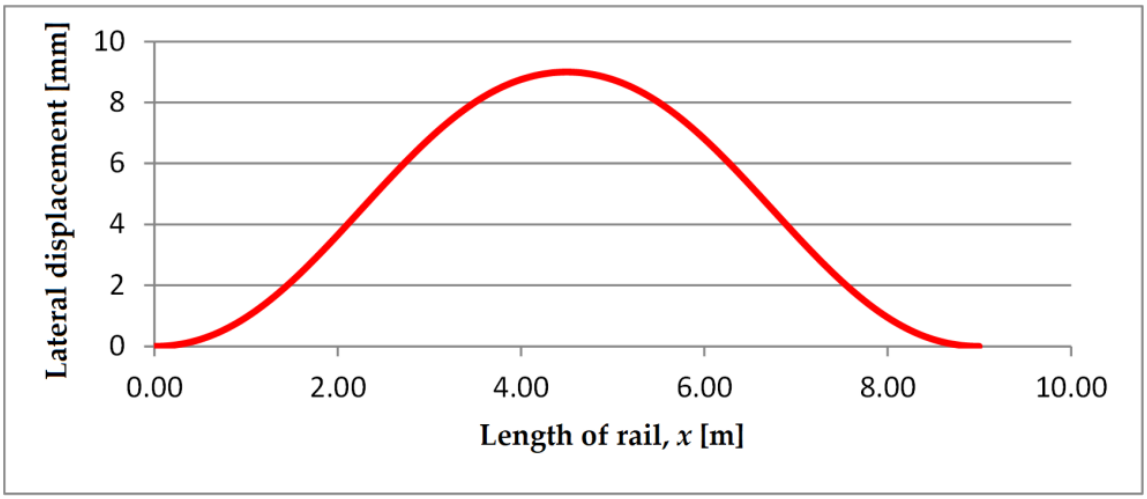



**Figure 14.** Lateral displacement of the examined section of rail.

As seen in the previous chapters, the rail section is inherently stable for a force lower than the thermal force $F_{cr}$, so in this case, a compressive force (thermal force) higher than the force $F_{cr}$ must be assumed. The structure becomes unstable for such a high compressive force, which is realized in increased lateral displacement beyond all limits.

If this is prevented by the applied lateral force $F_H$, the lateral displacement is stopped, and an equilibrium situation occurs. In the case of the present study, this occurs when the rail bolt or rib of the baseplate stops movement and can no longer shift. It will depend on the condition and dimensional tolerance of the anchors in the concrete sleeper.

In the present study, not only an initial error is considered, but also specific values of lateral displacement are taken into account (which can be formed in any case due to the high thermal force), and then an iteration method is used to find the magnitude of the force that can stabilize the system.

- The size of the initial imperfection was set to the minimum ($y_{k,max}$ = 1 mm) but was not neglected because of the consideration that there are always slight imperfections in a long, thin fabrication. No bending moment is generated in the rail from a support; its shape is bent by the initial defect, and the rail is stress-free.
- The lateral displacement was found to be a function of the wavelength of the distortion ($y_{max} = l/1000$). It is because large lateral displacements cannot occur for small wavelengths, simply just due to the inherent bending stiffness of the rail.
- The values of length of distortions ($l_{dist} \leq 3.0$ m), which were stable in the authors' previous tests, are out of the scope of investigation now; no lateral support is needed here, and the rail section is stable even under the effect of the maximum thermal force.

The results are shown in Tables 6 and 7. A positive value means the rail is stable, so it needs extra compression force (active force) to reach the required deflection value in the middle of the distortion. These values are, therefore, irrelevant because no such force is active in the track. However, for the cells colored red, the result is relevant, showing the lateral support required to prevent buckling.

**Table 6.** Lateral support requirements for rail 54E1 [kN] for different lengths of distortions and longitudinal compressive forces in the case $y_{k,max}$ = 1 mm, and $y_{max} = l/1000$.

| ΔT | F | Wavelength of Distortion [m] | | | | | | | | | |
|---|---|---|---|---|---|---|---|---|---|---|---|
| [°C] | [kN] | 3.6 | 4.2 | 4.8 | 5.4 | 6.0 | 6.6 | 7.2 | 7.8 | 8.4 | 9.0 |
| 5 | 83.7 | 6.26 | 4.81 | 3.42 | 2.75 | 2.11 | 1.75 | 1.40 | 1.18 | 0.98 | 0.83 |
| 10 | 167.5 | 6.00 | 4.54 | 3.18 | 2.50 | 1.87 | 1.51 | 1.17 | 0.95 | 0.75 | 0.60 |
| 15 | 251.2 | 5.74 | 4.27 | 2.93 | 2.25 | 1.64 | 1.27 | 0.93 | 0.71 | 0.52 | 0.37 |
| 20 | 334.9 | 5.48 | 4.01 | 2.68 | 2.00 | 1.40 | 1.03 | 0.70 | 0.48 | 0.29 | 0.14 |
| 25 | 418.6 | 5.22 | 3.74 | 2.44 | 1.75 | 1.16 | 0.79 | 0.47 | 0.24 | 0.06 | –0.09 |
| 30 | 502.4 | 4.96 | 3.47 | 2.19 | 1.50 | 0.92 | 0.55 | 0.24 | 0.01 | –0.17 | –0.32 |
| 35 | 586.1 | 4.70 | 3.20 | 1.95 | 1.25 | 0.69 | 0.31 | 0.01 | –0.22 | –0.40 | –0.55 |
| 40 | 669.8 | 4.44 | 2.94 | 1.70 | 1.00 | 0.45 | 0.07 | –0.22 | –0.46 | –0.63 | –0.78 |
| 45 | 753.6 | 4.18 | 2.67 | 1.45 | 0.75 | 0.21 | –0.17 | –0.46 | –0.69 | –0.87 | –1.01 |

**Table 7.** Lateral support requirements for rail 54E1 [kN] for different lengths of distortions and longitudinal compressive forces in the case $y_{k,max}$ = 2 mm, and $y_{max} = l/1000$.

| ΔT | F | Wavelength of Distortion [m] | | | | | | | | | |
|---|---|---|---|---|---|---|---|---|---|---|---|
| [°C] | [kN] | 3.6 | 4.2 | 4.8 | 5.4 | 6.0 | 6.6 | 7.2 | 7.8 | 8.4 | 9.0 |
| 5 | 83.7 | 6.21 | 4.75 | 3.38 | 2.71 | 2.08 | 1.71 | 1.37 | 1.15 | 0.96 | 0.80 |
| 10 | 167.5 | 5.89 | 4.44 | 3.09 | 2.42 | 1.80 | 1.44 | 1.11 | 0.89 | 0.70 | 0.55 |
| 15 | 251.2 | 5.57 | 4.12 | 2.80 | 2.13 | 1.53 | 1.17 | 0.85 | 0.63 | 0.45 | 0.30 |
| 20 | 334.9 | 5.25 | 3.80 | 2.51 | 1.85 | 1.26 | 0.90 | 0.59 | 0.37 | 0.19 | 0.05 |
| 25 | 418.6 | 4.94 | 3.48 | 2.23 | 1.56 | 0.99 | 0.63 | 0.33 | 0.11 | –0.06 | –0.20 |
| 30 | 502.4 | 4.62 | 3.16 | 1.94 | 1.27 | 0.72 | 0.36 | 0.07 | –0.15 | –0.32 | –0.46 |
| 35 | 586.1 | 4.30 | 2.85 | 1.65 | 0.98 | 0.45 | 0.09 | –0.19 | –0.41 | –0.57 | –0.71 |
| 40 | 669.8 | 3.99 | 2.53 | 1.36 | 0.69 | 0.18 | –0.19 | –0.45 | –0.67 | –0.83 | –0.96 |
| 45 | 753.6 | 3.67 | 2.21 | 1.07 | 0.40 | –0.10 | –0.46 | –0.71 | –0.93 | –1.09 | –1.21 |

The calculated values are small so that the rail fastening can support the rail laterally, at least at the calculated distortion lengths. However, the "wobbly", manually movable baseplates cannot even provide this force, only in their end position, so the rail moves freely between the end positions of the baseplate due to the thermal force, causing a gauge narrowing.

## 6. Conclusions

The results and conclusions drawn thereof are summarized as follows.

Analysis of the results of the measurement trains shows that gauge narrowing is typical for straight sections; it is not generated in curved tracks.

- On straight track sections, the track gauge of the old 48 kg/m rail-system superstructures has narrowed by 0.15–0.25 mm/year over time. Regarding gauge narrowing, the MÁV48.5 rail-system superstructure is the most affected. The explanation is that these superstructures are old, and 50–55-year-old structures are quite common on the main lines, and the aging processes are already increasing. In straight sections, the gauge narrows as time progresses. The most affected are the concrete sleepers originally built with wooden inserts marked "*T-type*", and "*L-type*" and for MÁV48 rail system, where the aging of the wooden inserts and the ingress of water into the dowels initiate a serious deterioration process.
- Finite element modeling has shown that the sleeper's shrinkage and other time-dependent deformation do not contribute significantly to the development of the gauge narrowing. The maximum magnitude of the time-dependent effects remains below 1.0 mm. With time-dependent effects, central transfer of wheel loads, and proper support of the cross sleepers—careful maintenance—the cumulative rate of gauge narrowing is also around or below 1 mm, i.e., insignificant. However, the uneven support of the cross sleepers and the eccentric transfer of wheel loads to the sleeper can cause a gauge narrowing of up to 7.39 mm. The cumulative values of these effects can lead to significant gauge narrowing of 8–9 mm. With careful design and maintenance, high narrowing values can be avoided by ensuring adequate and uniform support of the concrete sleepers.
- In the case of loss of function of the rail fastenings, if 10 fastenings fail laterally for 54E1 rails and 11 fastenings fail for 60E1 rails, the force generated in the rail by the temperature rise exceeds the critical compression force for buckling, and the rail is not stable. However, for shorter lengths without support, the rail remains stable. Baseplates that do not provide sufficient lateral support can move freely only to a certain extent and then hit the rail bolt, thus providing lateral support—but with a narrower gauge. With an initial misalignment of 1 mm and the wavelengths and compressive forces in the rail shown in Tables 6 and 7, it was found that even small lateral forces can stabilize the rail and support it laterally.

**Author Contributions:** Conceptualization, P.B., N.L., Á.V. and S.F.; methodology, P.B., N.L., Á.V. and S.F.; software, P.B., N.L., Á.V. and S.F.; validation, P.B., N.L., Á.V. and S.F.; formal analysis, P.B., N.L., Á.V. and S.F.; investigation, P.B., N.L., Á.V. and S.F.; resources, P.B., N.L., Á.V. and S.F.; data curation, P.B., N.L., Á.V. and S.F.; writing—original draft preparation, P.B., N.L., Á.V. and S.F.; writing—review and editing P.B., N.L., Á.V. and S.F.; visualization, P.B., N.L., Á.V. and S.F.; supervision, P.B., N.L., Á.V. and S.F.; project administration, P.B., N.L., Á.V. and S.F.; funding acquisition, P.B., N.L., Á.V. and S.F. All authors have read and agreed to the published version of the manuscript.

**Funding:** This research received no external funding.

**Data Availability Statement:** Not applicable.

**Acknowledgments:** The authors would like to thank MÁV Ltd. and MÁV CRTI Ltd. for their help with providing measuring data. This paper was prepared by the cooperation of research teams "BME-RAIL" and "SZE-RAIL". The authors also thank the technical support of J. Lógó, G. Pintyőke, D.B. Merczel, and G. Kormos.

**Conflicts of Interest:** The authors declare no conflict of interest.

## Nomenclature

| Symbols | Description (Meaning) | Units |
|---|---|---|
| $\rho(x)$ | radius of the elastic beam at the abscissa ($x$) | m |
| $\overline{x}_{TG,i}$ | the track gauge value at the $i$-th measurement point | mm |
| $\overline{x}_{TG}$ | the average of the individual values of the track gauge | mm |
| $A$ | cross-sectional area of the rail | $mm^2$ |
| $C$ | bedding modulus (bedding factor) below the sleeper's bottom | $N/mm^3$ |
| $E$ | modulus of elasticity of the rail steel, $E$ = 215,000 $N/mm^2$ | $N/mm^2$ |
| $F_{comp}$ | longitudinal compression force | kN |
| $F_{cr}$ | critical force inducing buckling of the track | kN |
| $F_H$ | horizontal lateral force of support acting on the rail | kN |
| $I$ | moment of inertia of the cross-section of the rail | $mm^4$ |
| $I_y$ | lower moment of inertia of the cross-section of the rail | $mm^4$ |
| $k$ | sleeper spacing | m |
| $l_{dist}$ | wavelength of the distortion | mm |
| $L_{lrb}$ | length of the longitudinal replacement beam | mm |
| $l_{ws}$ | length of the rail without lateral support | m |
| $M(x)$ | bending moment generated in the beam due to initial geometrical distortion | Nmm |
| $Q$ | axle load of the vehicle | kN |
| $s$ | width of the longitudinal substitutional beam | mm |
| $S_{TG}$ | the value of the cumulative deviation from the mean at a given measurement point '$i$' | mm |
| $t$ | factor depending on the required safety | — |
| $V$ | speed | km/h |
| $x$ | *x-direction* based on Figures 6 and 7 | – |
| $x_{dist}$ | absolute distance from the cross-section | mm |
| $xx$ | *xx-direction* based on Figures 6 and 7 | – |
| $y$ | *y-direction* based on Figures 6 and 7 | – |
| $Y$ | horizontal lateral force | kN |
| $y_k$ | initial geometrical distortion | mm |
| $y_{k,max}$ | maximum value of the initial geometrical distortion | mm |
| $Y_{max}$ | maximum value of horizontal lateral force | kN |
| $Y_{max,sleeper}$ | maximum value of horizontal lateral force acting on one sleeper | kN |
| $yy$ | *yy-direction* based on Figures 6 and 7 | – |
| $Z$ | wheel load of the vehicle | kN |
| $z$ | *z-direction* based on Figures 6 and 7 | – |
| $zz$ | *zz-direction* based on Figures 6 and 7 | – |
| $\alpha$ | coefficient of linear thermal expansion of the rail steel, $\alpha = 1.15 \times 10^{-5}$ 1/°C | 1/°C |
| $\beta$ | dynamic multiplication factor | — |
| $\delta$ | factor depending on the quality of the superstructure | — |
| $\Delta T$ | deviation of the temperature of the rail from the actual neutral temperature | °C |
| $\eta$ | value of the influence line of deflection | — |
| $\lambda$ | coefficient dependent on the fixation of the end of the beam | — |
| $\sigma_f$ | yield strength of rail steel | $N/mm^2$ |
| $\tau(x)$ | angle of the tangent drawn to the geometry of the structure | — |
| $\varphi$ | speed-dependant factor | — |

## Abbreviations

| Abbreviation | Meaning |
|---|---|
| ANN | artificial neural network |
| CC | circular curve |
| CWR | continuously welded rail |
| EC | entire curve |
| EMD | Empirical Mode Decomposition |
| FAS | Fourier Amplitude Spectrum |
| ICP | iterative closest point |
| IMF | Intrinsic Mode Function |

| | |
|---|---|
| IoT | Internet of Things |
| IoT-DTG | Internet of Things enhanced digital track gauge |
| LCD | liquid crystal display |
| LED | light emitting diode |
| MÁV CRTI Ltd. | MÁV Central Rail and Track Inspection Ltd., Budapest, Hungary |
| MÁV or MÁV Ltd. | Hungarian State Railways Ltd., Budapest, Hungary |
| MGT | million gross tons |
| MSE | mean squared error |
| R&D | research and development |
| SVM | support vector regression |
| TC | transition curve |
| TEN-T | Trans-European Transport Network |
| TG | track gauge |
| TQI | Track Quality Index |
| UIC | International Union of Railways |
| VMD | Variational Mode Decomposition |
| WiFi | wireless fidelity |

## References


1. Czére, B. *A Vasút Története (The History of Railway—In Hungarian)*; Corvina Kiadó: Budapest, Hungary, 1989.
2. Nøland, J.K. Hydrogen Electric Airplanes: A Disruptive Technological Path to Clean up the Aviation Sector. *IEEE Electrif. Mag.* **2021**, *9*, 92–102. [CrossRef]
3. Atilhan, S.; Park, S.; El-Halwagi, M.M.; Atilhan, M.; Moore, M.; Nielsen, R.B. Green Hydrogen as an Alternative Fuel for the Shipping Industry. *Curr. Opin. Chem. Eng.* **2021**, *31*, 100668. [CrossRef]
4. Gáspár, L. Lifetime Engineering Principles and Durable Roads. *Int. J. Pavement Eng. Asph. Technol.* **2016**, *17*, 58–72.
5. Gáspár, L.; Bencze, Z. Increasing Life Expectancy of Road Pavements. *Gradjevinar* **2020**, *72*, 515–522. [CrossRef]
6. He, L.; Cai, H.; Huang, Y.; Ma, Y.; Van Den Bergh, W.; Gaspar, L.; Valentin, J.; Vasiliev, Y.E.; Kowalski, K.J.; Zhang, J. Research on the Properties of Rubber Concrete Containing Surface-Modified Rubber Powders. *J. Build. Eng.* **2021**, *35*, 101991. [CrossRef]
7. Szpotowicz, R.; Tóth, C. Revision of Sustainable Road Rating Systems: Selection of the Best Suited System for Hungarian Road Construction Using Topsis Method. *Sustainability* **2020**, *12*, 8884. [CrossRef]
8. Primusz, P.; Tóth, C. Use of the Modified Ramberg-Osgood Material Model to Predict Dynamic Modulus Master Curves of Asphalt Mixtures. *Materials* **2023**, *16*, 531. [CrossRef]
9. Fischer, S.; Harangozó, D.; Németh, D.; Kocsis, B.; Sysyn, M.; Kurhan, D.; Brautigam, A. Investigation of Heat-Affected Zones of Thermite Rail Weldings. *Facta Univ. Ser. Mech. Eng.* 2023. [CrossRef]
10. Fischer, S.; Németh, D.; Horváth, H. Investigation of the Track Gauge in Curved Sections, Considering Hungarian Railway Lines. *Infrastructures* **2023**, *8*, 69. [CrossRef]
11. Fischer, S.; Liegner, N.; Bocz, P.; Vinkó, Á.; Terdik, G. Investigation of Track Gauge and Alignment Parameters of Ballasted Railway Tracks Based on Real Measurements Using. *Infrastructures* **2023**, *8*, 26. [CrossRef]
12. Németh, D.; Horváth, H.; Rad Movahedi, M.; Németh, A.; Fischer, S. Investigation of the Track Gauge in Straight Sections, Considering Hungarian Railway Lines. *Acta Polytech. Hung.* **2022**, *19*, 155–156. [CrossRef]
13. Nugymanova, G.; Nurgaliyeva, M.; Zhanbirov, Z.; Naumov, V.; Taran, I. Choosing a Servicing Company's Strategy While Interacting with Freight Owners at the Road Transport Market. *Sci. Bull. Natl. Min. Univ.* **2021**, *1*, 204–210. [CrossRef]
14. Ramazan, B.; Mussaliyeva, R.; Bitileuova, Z.; Naumov, V.; Taran, I. Choosing the Logistics Chain Structure for Deliveries of Bulk Loads: Case Study of the Republic Kazakhstan. *Natsional'nyi Hirnychyi Universytet. Nauk. Visnyk* **2021**, *18*, 142–147. [CrossRef]
15. Macura, D.; Laketić, M.; Pamučar, D.; Marinković, D. Risk Analysis Model with Interval Type-2 Fuzzy FMEA—Case Study of Railway Infrastructure Projects in the Republic of Serbia. *Acta Polytech. Hung.* **2022**, *19*, 103–118. [CrossRef]
16. Weinberg, S.J.; Sanches, F.; Ide, T.; Kamiya, K.; Correll, R. Supply Chain Logistics with Quantum and Classical Annealing Algorithms. *Sci. Rep.* **2022**, *13*, 4770. [CrossRef] [PubMed]
17. Yingfei, Y.; Mengze, Z.; Zeyu, L.; Ki-Hyung, B.; Andriandafiarisoa Ralison Ny Avotra, A.; Nawaz, A. Green Logistics Performance and Infrastructure on Service Trade and Environment-Measuring Firm's Performance and Service Quality. *J. King Saud. Univ. Sci.* **2022**, *34*, 101683. [CrossRef]
18. *EN 13848-1: Railway Applications—Track—Track Geometry Quality—Part 1: Characterisation of Track Geometry*; CEN European Committee for Standardization: Brussels, Belgium, 2008.
19. Chandra, S.; Agarwal, M.M. *Railway Engineering*, 2nd ed.; Oxford University Press: New Delhi, India, 2015.
20. Tzanakakis, K. History of the Track Gauge. In *The Railway Track and Its Long Term Behaviour*; Springer Tracts on Transportation and Traffic; Springer: Berlin/Heidelberg, Germany, 2013; Volume 2, ISBN 9783642360503.
21. Monfort, A. The Track Gauge in Spain: The Endless History. *Rev. Obras Publicas* **2019**, *166*, 64–75.
22. Puffert, D.J. The Standardization of Track Gauge on North American Railways, 1830–1890. *J. Econ. Hist.* **2000**, *60*, 933–960. [CrossRef]

23. Puffert, D.J. Path Dependence in Spatial Networks: The Standardization of Railway Track Gauge. *Explor. Econ. Hist.* **2002**, *39*, 282–314. [CrossRef]
24. Wang, C.; Li, X.; Chen, P.; Xie, Y.; Liu, W. Spatial Pattern and Developing Mechanism of Railway Geo-Systems Based on Track Gauge: A Case Study of Eurasia. *J. Geogr. Sci.* **2020**, *30*, 1283–1306. [CrossRef]
25. Zheng, S.; Peng, L.; Zhong, Q.; Li, L. Gauge and Wear Detection Method for Portable Track Inspection Trolley. *Zhendong Ceshi Yu Zhenduan/J. Vib. Meas. Diagn.* **2022**, *42*, 600–605. [CrossRef]
26. Pay, Z.H.; Ng, A.K.; Zhang, Z.A. Design and Fabrication of an Internet of Things Enhanced Digital Track Gauge. In Proceedings of the 8th International Conference on Control, Automation and Robotics, ICCAR 2022, Xiamen, China, 8–10 April 2022; IEEE: New York, NY, USA, 2022; pp. 45–48.
27. Yilmazer, M.; Karakose, M.; Aydin, I. Determination of Railway Track Gauge with Image Processing. In Proceedings of the 2021 International Conference on Data Analytics for Business and Industry, ICDABI 2021, Virtual, Online, 25–26 October 2021; IEEE: New York, NY, USA, 2021; pp. 510–514.
28. Zhang, G.; Ma, Z.; Yuan, J.; Kang, D.; Yan, D.; Li, J. Track Gauge Measurement Based on Wheel-Rail Lateral Relative Displacement. *Guangdian Gongcheng/Opto-Electron. Eng.* **2020**, *47*, 190252. [CrossRef]
29. Shi, H.; Xu, M.; Yu, Z. Track Gauge Measurement Method Based on Least-Square Curve Fitting Theory. *Tiedao Xuebao/J. China Railw. Soc.* **2019**, *41*, 81–88. [CrossRef]
30. Tsubokawa, Y.; Ishikawa, T. Development of a Dynamic Track Measuring Device for Gauge and Twist to Reduce Derailment Accidents. *WIT Trans. Built Environ.* **2018**, *181*, 253–262. [CrossRef]
31. Tang, W.B.; Long, Y.H.; Xie, Y.J.; Li, H.J.; Tang, C.B.; Zhang, Z.X. A Channel Rail Gauge Detection System of Modern Tram. In Proceedings of the 15th IEEE International Conference on Networking, Sensing and Control (ICNSC 2018), Zhuhai, China, 27–39 March 2018; IEEE: New York, NY, USA, 2018; pp. 1–5.
32. Aharkov, O.V.; Tverdomed, V.M.; Boiko, V.D.; Kovalchuk, V.V.; Strelko, O.H. Influence of the Structural Design of Rail Fastenings on Ensuring the Stability of Track Gauge in Operating Conditions. In Proceedings of the IOP Conference Series: Materials Science and Engineering—8th International Scientific Conference on Reliability and Durability of Railway Transport Engineering Structures and Buildings, TRANSBUD 2019, Kharkiv, Ukraine, 20–22 November 2019; Volume 708, p. 012001.
33. Ahac, M.; Lakusic, S. Tram Track Maintenance-Planning by Gauge Degradation Modelling. *Transport* **2015**, *30*, 430–436. [CrossRef]
34. Akkerman, G.; Akkerman, S. Rail Gauge Trajectory, Macro and Micro Profile of Tracks. In Proceedings of the IOP Conference Series: Materials Science and Engineering—8th International Scientific Conference Transport of Siberia 2020, Novosibirsk, Russia, 22–27 May 2020; Volume 918, p. 012153.
35. Falamarzi, A.; Moridpour, S.; Nazem, M.; Cheraghi, S. Prediction of Tram Track Gauge Deviation Using Artificial Neural Network and Support Vector Regression. *Aust. J. Civ. Eng.* **2019**, *17*, 63–71. [CrossRef]
36. Hungarian State Railways D.54, Construction and Track Maintenance Technical Data, Regulations. 1988. Available online: https://www.mavcsoport.hu/mav-csoport/bemutatkozas/szabvanykozpont (accessed on 2 June 2023).
37. European Committee for Standardization EN 206:2013+A2:2021: Concrete—Specification, Performance, Production and Conformity. 2021, pp. 1–103. Available online: https://genorma.com/en/project/show/cen:proj:73198 (accessed on 2 June 2023).
38. European Committee for Standardization EN 10138-2:2005: Prestressing Steels—Part 2: Wire. 2005, pp. 1–15. Available online: https://global.ihs.com/doc_detail.cfm?item_s_key=00496117 (accessed on 2 June 2023).
39. Esveld, C. *Modern Railway Track*; MRT Production: Zaltbommel, The Netherlands, 2001; ISBN 978-1-326-05172-3.
40. Lichtberger, B. *Track Compendium*; Eurailpress Tetzlaff-Hestra GmbH & Co. Publ.: Hamburg, Germany, 2005.
41. Fischer, S.; Eller, B.; Kada, Z.; Németh, A. *Railway Construction*; Universitas-Győr Nonprofit Kft.: Gyor, Hungary, 2015; ISBN 978-615-5298-69-1.
42. European Committee for Standardization EN 1992-1-1:2004/A1:2014: Design of Concrete Structures—Part 1-1: General Rules and Rules for Buildings. 2014, pp. 1–226. Available online: https://infostore.saiglobal.com/en-us/standards/en-1992-1-1-2004-a1-2014-333210_saig_cen_cen_765732/ (accessed on 2 June 2023).
43. Hungarian State Railways D.12/H, Instruction for the Construction, Maintenance and Supervision of CWR Tracks. 2009, pp. 1–123. Available online: https://www.mavcsoport.hu/mav-csoport/bemutatkozas/szabvanykozpont (accessed on 2 June 2023).


**Disclaimer/Publisher's Note:** The statements, opinions and data contained in all publications are solely those of the individual author(s) and contributor(s) and not of MDPI and/or the editor(s). MDPI and/or the editor(s) disclaim responsibility for any injury to people or property resulting from any ideas, methods, instructions or products referred to in the content.